Investigation of the Pre-Ejection Period as a Marker for Sympathetic Activity during Acute Psychosocial Stress

Bachelor's Thesis in Medical Engineering

submitted
by

Sebastian Stühler

born 24.07.2001 in Ochsenfurt

Written at

Machine Learning and Data Analytics Lab
Department Artificial Intelligence in Biomedical Engineering
Friedrich-Alexander-Universität Erlangen-Nürnberg (FAU)

in Cooperation with

Chair of Health Psychology

Advisors: Luca Abel M. Sc., Robert Richer M. Sc., Prof. Dr. Bjoern Eskofier, Prof. Dr. Nicolas Rohleder

Started: 15.12.2022

Finished: 15.05.2023

Ich versichere, dass ich die Arbeit ohne fremde Hilfe und ohne Benutzung anderer als der angegebenen Quellen angefertigt habe und dass die Arbeit in gleicher oder ähnlicher Form noch keiner anderen Prüfungsbehörde vorgelegen hat und von dieser als Teil einer Prüfungsleistung angenommen wurde. Alle Ausführungen, die wörtlich oder sinngemäß übernommen wurden, sind als solche gekennzeichnet.
Die Richtlinien des Lehrstuhls für Bachelor- und Masterarbeiten habe ich gelesen und anerkannt, insbesondere die Regelung des Nutzungsrechts.

Erlangen, den 15. Mai 2023

Übersicht

Der negative Einfluss von chronischem Stress auf die meschliche Gesundheit ist weitreichend untersucht. Häufig genutzte Messmethoden, wie die Herzrate oder die Herzratenvariabilität bieten allerdings nicht die Möglichkeit die Einflüsse des sympathischen Nervensystems isoliert zu messen. In der menschlichen Stressreaktion ist das sympathische Nervensystem für kurzfristige Anpassungen verantwortlich und trägt zu einem erheblichen Teil zur gesamten Stressreaktion bei. Eine vielversprechende Methode um die isolierte Messung sympathischer Aktivität durchzuführen, ist die Pre-Ejection Period (PEP). Dazu muss der Beginn der Q-Welle im Elektrokardiogramm und der B-Punkt im Impedanzkardiogramm detektiert werden. Insbesondere die Detektion des B-Punktes stellt sich als besonders herausfordernd dar, da sich die Ausprägung dieses Punktes zwischen vesrchiedenen Personen und auch innerhalb einer Person ändern kann. In der Literatur werden einige automatische Detektionsalgorithmen vorgestellt, deren Genauigkeit allerdings zu hinterfragen ist.

Um diesen Zweifeln entgegenzuwirken wurden in dieser Arbeit drei Algorithmen um den Startpunkt der Q-Welle zu berechnen, vier Algorithmen zum extrahieren der Position des B-Punktes und zwei Methoden zur Korrigierung von Ausreißern implementiert. Anschließend wurden alle Algorithmen zur Berechnung des Beginns der Q-Welle mit allen Algorithmen zum extrahieren des B-Punktes, sowie mit den Methoden zum Korrigieren der Ausreißer kombiniert. Um die Algorithmen auf deren Genauigkeit zu überprüfen, wurden im Rahmen dieser Bachelorarbeit 5086 Herzschläge manuell annotiert und als Referenzwert für weitere Untersuchungen genutzt.

Die Analyse der Algorithmen zeigte, dass die Ergebnisse früherer Untersuchungen in dieser Arbeit nicht bestätigt werden konnten. In zugehöriger Literatur hat ein Algorithmus, basierend auf diversen Entscheidungsregeln und schwellenwertbasierter Auswahl relevanter Punkte, mit einer anschließenden Ausreißerkorrektur durch ein autoregressives Modell am besten abgeschnitten. Die im Rahmen dieser Arbeit erzeugten Ergebnisse wiederlegen die herausstechende Leistung des besagten Algorithmus. Eine weitere Methode basierte, auf der Detektion des lokalen Minimums in der zweiten Ableitung des Impedanzkardiogrammsignals und anschließender Ausreißerkorrektur durch ein autoregressives Modell. Beim Vergleich mit den manuell annotierten Referenzdaten konnte in Kombination mit einer Methode, die zur Schätzung des Startpunktes der PEP $40\,\text{ms}$ von der R-Zacke abzieht, der geringste mittlere Fehler von $15.31 \pm 19.20\,\text{ms}$ erzielt werden.

Abstract

The negative impact of chronic stress on the individual's health is well understood. However, current non-invasive methods for stress measurement, such as heart rate (HR), or heart rate variability (HRV), cannot reflect the sympathetic drive to the heart in isolation. The sympathetic nervous system (SNS) is responsible for short term responses and has a major influence on the human stress response. A promising method to measure sympathetic activity in isolation is the PEP. This time period starts at the Q-wave onset in the electrocardiogram (ECG) and ends at the B-point in the impedance cardiogram (ICG). In particular, the detection of the B-point is challenging since the morphology of this point varies between and even within individuals. Automatic event detection algorithms, to extract the points necessary for PEP computation have been proposed in related work. However, previous investigations indicate that their accuracy is questionable.

To counteract these uncertainties, three methods for Q-wave onset (Q-onset) detection, four methods to extract the B-point, and two algorithms for outlier correction were implemented in this work. Subsequently, all algorithms for Q-onset detection were combined with all algorithms for B-point extraction, and outlier correction. To verify the accuracy of the implemented algorithms, 5086 cardiac cycles were manually labeled in this work and used as a reference for further investigations.

The results obtained in this work, could not confirm previous findings. An algorithm based on multiple decision rules, thresholds, and a subsequent outlier correction with an autoregressive model to extract the B-point, was proposed to show superior performance in related work. However, in this work, a PEP computation pipeline using a method based on subtracting 40 ms from the R-peak for Q-onset detection and the local minimum in the second derivative of the cardiac impedance ($\boldsymbol{dZ^2/dt^2}$) signal with subsequent outlier correction, showed the least mean absolute error (MAE) of 15.31 ± 19.20 ms with respect to the manually labeled reference data.

Contents

Chapter 1

Introduction

Many situations in our daily lives can cause psychosocial stress. These include traffic jams, the fear of failure and its consequences, poverty, or environmental factors such as natural disasters [Doe21]. Although stress helps us to respond to a threat in an appropriate way, becoming chronically stressed can affect our health negatively [McE17]. Several diseases like cardiovascular dysfunction, diabetes, and autoimmune syndromes are linked to chronic stress [Mar15].

When an individual is experiencing acute psychosocial stress, the physical response of the body is based on two main pathways. Short term responses such as an increase in alertness are controlled by the SNS. The slower reacting Hypothalamus-pituitary-adrenal (HPA) axis evokes an intensified and prolonged response to stress [Doe21]. Since the SNS has a major influence on the human stress response, reliable SNS markers are highly relevant [Dro22]. However, current noninvasive methods such as the measurement of HR, HRV or arterial blood pressure are unable to reflect sympathetic activity isolated [Dro22; New79]. Therefore, there is a need for novel stress markers that circumvent this limitation. One promising marker is the PEP, which is proposed as the best noninvasive method for assessing the sympathetic control of the heart in related work [Cac94; Dro22]. PEP is defined as the time interval from the start of ventricular depolarization to the beginning of blood ejection from the ventricle [New79; For18; Sha19]. Thus, the gold standard approach to detect the events, necessary for PEP computation is the synchronized measurement of the ECG and the ICG [She90; Lie13]. From the ECG, the start point of PEP can be obtained by detecting the Q-wave onset, which corresponds to the beginning of ventricular depolarization [Pil23]. The end point of PEP can be determined indirectly from the ICG, by extracting the B-Point from the signal of the first derivative of the cardiac impedance (dZ/dt), which indicates the before mentioned beginning of blood ejection from the ventricle [She90].

Since both the detection of the Q-wave onset and the detection of the B-Point are sensitive to noise and prone to artifacts, reliable computation of PEP by automatic algorithms is challenging [Dro22]. Especially detecting the B-Point is difficult, as respiration, body movements, and cardiovascular dysfunctions influence the shape of the dZ/dt signal. Hence, different dZ/dt waveforms between and even within individuals may occur [For18].

Several automatic event detection pipelines for PEP computation are therefore based on strong simplifications, which are prone to distortions and baseline shifts [She90; She22]. As a result, no common practice has been found in previous work and many publications lack information on the algorithms used, or the accuracy of the applied algorithms may be questioned [Árb17].

The goal of this bachelor's thesis is therefore to compare the performance of different event detection pipelines according to their accuracy in PEP computation. To determine the best performing event detection pipeline, data was collected in a study in the context of the EmpkinS collaborative research center [Emp23]. 40 participants performed the Trier Social Stress Test (TSST) for acute psychosocial stress induction [Kir93] and the control version of the Trier Social Stress Test (f-TSST) [Wie13] in randomized order on two consecutive days. Additionally to self-reports and biomarkers such as alpha-amylase or cortisol, which are gold standard measures to asses psychosocial stress, ECG and ICG data were recorded during the (f-)TSST. The captured data was used to compute PEP with different event detection pipelines and to generate a manually labeled gold standard. Thereby, the B-Points were marked according to a visual guideline stated by Árbol [Árb17] and examples of difficult-to-detect B-Points [For18]. Finally, the performance of the implemented event detection pipelines was evaluated, by comparison with the manually labeled reference data.

Chapter 2

Medical Background

The isolated noninvasive measurement of the sympathetic control of the heart is challenging. Typical measures, such as HR are often influenced by both vagal and beta-adrenergic activation [New79]. However, the parasympathetic nervous system (PNS) which is responsible for vagal activity has a greater influence on HR [Cac94]. To overcome this limitation and to allow isolated assessment of the SNS, which is responsible for beta-adrenergic activation, several cardiovascular measurement techniques have been introduced [New79]. Although the shortening of PEP is coincident with an increase in HR, HR does not affect PEP [Cac94]. This is because PEP, which is a systolic time interval is under the control of cardiac inotropy, which in turn is influenced by the positive inotropic effect of the SNS [Kro17]. Therefore PEP is known to be mainly directed by beta-adrenergic influences [Cac94]. To confirm this, several studies have been conducted using drugs to either stimulate or inhibit beta-adrenergic receptors and to block either the PNS or SNS to investigate influencing factors on PEP. The results revealed that the blockade of the PNS does not affect the duration of PEP. In all other cases, changes in PEP could be identified [Dro22]. Stimulation of beta-adrenergic receptors induced a decrease of PEP duration [Cac94; Dro22], whereas inhibition of beta-adrenergic receptors increased PEP [Dro22]. Furthermore, PEP was compared with changes in the T-wave amplitude, which should also reflect the sympathetic activity of the heart. T-wave amplitude was only influenced by beta-adrenergic manipulation. PEP, however, was sensitive to both beta- and alpha2-adrenergic changes [Dro22]. The results of the studies confirm that PEP is an accurate marker for sympathetic activation of the heart [New79] and outperforms the method based on changes in T-wave amplitude [Dro22].

PEP can be divided into two components. The electromechanical delay, which represents the duration from the ECG Q-wave to the beginning of the rising pressure in the left ventricle, and the isovolumic contraction. This time interval corresponds to the time until the pressure in the left ventricle is raised to the level that the aortic valve opens [Kro17; New79]. PEP

is therefore a noninvasive measure of all electrical and mechanical processes prior to the ejection of blood from the ventricle [New79]. The electromechanical delay is known to be fairly unaffected even under physiological and pathophysiological changes. This is the reason why its duration remains in a small range between 30 - 40 ms [Kro17]. Changes in PEP are therefore primarily caused by the isometric contraction time. Influencing factors are the contractility of the heart, changes in diastolic blood pressure (DBP), or other factors such as cardiac preload and afterload[Kro17; Cac94].

The term preload refers to the extent to which the ventricle is filled with blood during diastole. When the ventricle is packed, the muscle fibers in the myocardium stretch. This causes a sharp increase in contractility. Consequently, an increasing preload leads to a decrease in PEP duration [New79; Cac94; Kro17]. The counterpart to cardiac preload is cardiac afterload, which should produce the opposite effect [Bal18]. Cardiac afterload describes the resistance to left ventricular contraction [New79]. Therefore, for the aortic valve to open, the pressure in the left ventricle must exceed the pressure in the aorta. If the pressure in the aorta increases, more pressure must be built up in the ventricle, leading to a time delay. As a result, a prolongation of PEP can be obtained for an increase in cardiac afterload [New79]. The fact that cardiac preload and afterload affect PEP independently of the influence of the SNS can have a disturbing impact on psychophysiological examinations [New79; Kro17]. Other physiological and pathophysiological conditions that either prolong or shorten PEP have been found in previous studies. Age, negative inotropic agents, or blocking of the left bundle branch are known to increase the PEP duration [New79]. Factors such as exercise, psychosocial stress, pathologies of the aortic valve, acute hypoxemia, or the reaction to positive inotropic agents shorten PEP [New79].

Chapter 3

Related Work

Several algorithms for automatic PEP computation are proposed in related work. To introduce these methods, the chapter is divided into three parts. In the first two sections, frequently used methods to detect the Q-wave onset and the B-Point are discussed. The last section presents guidelines for manual labeling and emphasizes the continuing importance of manually labeled data for PEP evaluation.

Q-wave onset The Q-wave onset, which corresponds to the start of ventricular depolarization is well known as the starting point of PEP [She90]. Even if the point is physiologically the correct choice [Pil23], it is often not practical to use this point for automatic PEP computation [Ber04]. The fact that the Q-wave is not present in every patient's ECG, also when trying different electrode placements, is a major obstacle for using the Q-wave onset as starting point of PEP [She90; Ber04]. In these cases, other significant points such as the R-wave onset (R-onset) must be detected [She90; Ber04]. This leads to a between-subject variance, which severely limits the comparability of PEP [Ber04]. For this reason, several approaches have been developed to determine the timing of ventricular depolarization independent of the presence of a Q-wave.

Bernston et al. analyzed the ECG and ICG data of 30 healthy undergraduate students to compare the influence of the Q-onset and the R-onset as starting point of PEP [Ber04]. The participants could be equally divided into the following categories: those with an easily detectable Q-wave, those with a weak but scoreable Q-wave, and those with no Q-wave. The results of the analysis show, that using R-onset as the starting point leads to greater stability of PEP values across subjects with different Q-wave prominences and reduces the variance of manually labeled data from multiple raters. For this reason, Bernston et al. recommend using the R-onset as the starting point of PEP [Ber04].

Subtracting a fixed time interval from the R-peak provides an alternative method for estimating the location of the Q-wave onset [Lie13]. Previous work has shown that the

QR interval can be assumed to be nearly constant since it shows minimum change during physiological and psychological stress [Kro17; Pil23]. Therefore, a constant QR interval of 48 ms was used to estimate the Q-wave onset in previous work [Wil96; Bry08]. Since the validity of this method was not systematically assessed, Van Lien et al. conducted two studies to verify whether the proposed QR interval is appropriate. In total 132 healthy undergraduate students participated in the studies and were exposed to physical and psychological stressors in a laboratory and ambulatory setting. The results of the studies show that a QR interval of 40 ms is at least a good estimate for the Q-wave onset, even though it cannot replace its accurate detection [Lie13]. Furthermore, the findings of the studies are distinctive to the previously proposed QR interval of 48 ms, which turns out to be a poor estimate [Lie13].

R-peak detection is even simpler than the detection of the Q-onset and leads to the complete elimination of detection errors due to ambiguous Q-waves [See16]. To investigate the influence of using the RB interval instead of the QB interval for PEP computation, a study with 408 undergraduate students was conducted. To get even better insights into the composition of PEP Seery et al. evaluated the impact of the QR interval on total PEP additionally. The study revealed that the RB interval is responsible for 90% of the variance of PEP, while the QR interval is only responsible for a part of 10%. If we move away from absolute levels and look at PEP changes, the RB interval is responsible for an even greater part of 98%, whereas the QR interval contributes only 2%. The results show that the RB interval is a good estimate of PEP, especially when looking at PEP changes, which is the more significant marker in psychology [Ber04; See16]. The fact that the R-peak is easy to extract and therefore more reliable than the detection of the Q-onset is a clear advantage of this method [Lie13; Kor18]. This simplicity may explain the frequent use of the R-peak for PEP computation [Kro17; Bal18; Kor18; Dro22; She22].

B-point Accurate automatic detection of the B-point is known to be difficult due to the high inter- and intra-subject variability in the dZ/dt waveform [Árb17; For18]. Thus, manual labeling, which is a very time-consuming process is still required to determine the correct B-point [For18]. Therefore, the systematic assessment of the performance of common B-point detection algorithms is highly relevant [Árb17].

Debski et al. investigated the B-point detection accuracy of algorithms based on the inflection point of the second derivative and the maximum peak of the third derivative using manually labeled reference data. A study with 21 healthy college students revealed the similar performance of the two algorithms. However, Debski et al. recommend which algorithm should be applied for which dZ/dt waveform. Accordingly, for signals with a visible inflection point, the method based on the second derivative is suggested. For signals where no inflection point is recognizable, the algorithm based on the third derivative is more applicable [Deb93].

Putting the Initial Systolic Time Interval (ISTI) in a quadratic equation has been proposed to estimate the B-point relative to the R-peak in related work [Loz07; Mei07]. The advantage of this method is that the B-point can be estimated from the R-peak and the maximum of the dZ/dt signal, which are the most prominent points in the ECG and dZ/dt waveforms [Lie13]. To verify the validity of this method, Van Lien et al. conducted two studies as mentioned in the previous section. Compared with previous findings, Van Lien et al. found different parameters for the regression equation in both studies. Also, the high agreement of the estimated RB interval with the variance of the true RB interval of 95% obtained in prior studies could not be confirmed by Van Lien et al. with an agreement of 79% and 81%, respectively. Nevertheless, the ISTI may be useful to assist in the detection of the actual B-Point [Lie13].

In another study, Árbol et al. investigated the performance of frequently used detection methods based on cycle-by-cycle isoelectric crossings, the maxima of the second derivative, and the maxima of the third derivative, by comparing their results with a manually labeled gold standard. Additionally, Árbol et al. performed literature research regarding the usage of automatic B-Point detection algorithms. Since only the algorithm based on the third derivative has shown acceptable results and 78% of the articles do not specify, which algorithm they used, Árbol et al. criticize the accuracy of the already obtained results, as well as the missing ability of reproduction [Árb17].

Various algorithms, which have been used to detect the B-Point were relying on fixed rules. To improve the performance of these algorithms, ensemble averaging is often performed [For18]. However, using this method reduces the temporal resolution, and difficulties in the detection of the B-Point may persist [Lie13; For18].

Forouzanfar et al. developed a novel automatic algorithm for beat-to-beat B-Point extraction to circumvent this limitation. Therefore, the B-Point detection pipeline consists of several steps, such as limiting the search interval and a threshold-based point selection. Furthermore, an autoregressive model is included for outlier correction. These steps make the algorithm less prone to noise and artifacts. Other commonly used B-Point detection algorithms based on the zero crossing of the dZ/dt signal, the reversal point of the dZ/dt signal, and the maximum of the third derivative of the ICG signal were also implemented. In a study with 20 healthy participants, the accuracy of the implemented algorithms compared with a manually labeled gold standard was evaluated. As a result, the superior performance of the novel automatic algorithm was revealed, as it showed the lowest deviation from the reference data [For18].

Finally, Sheikh et al. developed a novel data-driven machine learning approach to determine the location of the B-Point. In a study with 189 participants, the novel algorithm was compared with five state-of-the-art B-Point detection algorithms. The results of this study showed, that the machine learning approach outperformed the commonly used detection algorithms, which were either based on fixed rules (zero crossing, second derivative rule,

and third derivative rule [Árb17]) or data-driven approaches (linear and quadratic regression equation [Loz07]). Furthermore, the varying performance of the proposed algorithm in different conditions such as neutral or stress was found. Sheikh et al. explained this finding by the general limitation of data-driven algorithms that training and test data must contain all possible expressions [She22].

Manual Labeling Automatic B-Point detection algorithms are known to be prone to noise and artifacts [Dro22]. Hence, generating reliable results is not possible by often used state-of-the-art algorithms [Árb17]. As manual labeling is still the gold standard to pinpoint the accurate B-Point location and is of great importance to assess the performance of several B-Point detection algorithms, some guidelines for manual labeling have been elaborated in related work [Lie13; For18].

Nagel et al. proposed, that physiological changes of the dZ/dt waveform and distorting influences such as noise, reduce the precision and reliability of extracted B-Points [Nag89]. To counteract this limitation Sherwood et al. proposed guidelines for visual B-Point detection. According to the definition of Sherwood et al., the B-Point corresponds to the beginning of the rapid rise to the maximum peak of the dZ/dt signal and typically lies close to the zero-line of the dZ/dt signal [She90]. As part of a study to assess the performance of different B-Point detection algorithms, Árbol et al. developed a visual guideline to provide objective instruction for B-Point detection. The proposed decision tree is based on the previous work of Nagel et al. and Sherwood et al. and includes various morphologies of the dZ/dt signal [Árb17].

Chapter 4

Methods

To investigate the effects of psychosocial stress on several health-related parameters such as respiratory rate, HR, or PEP, a study was conducted at the *Machine Learning and Data Analytics Lab* from December 2022 to May 2023. The participants were asked to perform the TSST and f-TSST in randomized order on two consecutive days. In order to obtain a balanced dataset, the order of the TSST and f-TSST was alternated weekly. In addition, the participants were divided into a standing and sitting group.

4.1 Study Population

Further information regarding the 15 participants (9 female and 6 male), which have been selected for the analysis in this work is provided in the following paragraph. The demographic and anthropometric data of the subjects are listed in Table 4.1. Participants were recruited via

Table 4.1: Demographic and anthropometric data of the participants; Mean $\pm$ SD

	Age [years]	**Height** [cm]	**Weight** [kg]	**BMI** [$\mathrm{kg\,m^{-2}}$]
Female	24.11 ± 2.51	168.33 ± 5.50	59.44 ± 6.06	20.92 ± 1.14
Male	21.50 ± 1.61	180.83 ± 5.43	76.50 ± 10.69	23.35 ± 2.79
Total	23.07 ± 2.54	173.33 ± 8.21	66.27 ± 11.73	21.89 ± 2.30

mail distribution lists, social media, flyer notices, and in person. Eligibility for the study was assessed in advance using a screening questionnaire. In the process, those who met at least one of the following conditions were excluded: age below 18 or above 50 years, non-German native language, a BMI lower than 18 or higher than 30, physical or mental illnesses of any kind, medication intake, smoking, drug use, adiposity, and experience with a comparable stress test. As an expense allowance, the participants either received 50 € or could choose 5 *Versuchspersonenstunden* as compensation, if they were psychology students.

4.2 Stress Induction

For psychosocial stress induction, the TSST was used [Kir93]. Due to the combination of social evaluation, a mental arithmetic task, and the unpredictability of the upcoming event, the TSST is known to be an effective stressor that leads to a significant activation of the HPA axis [All17]. Therefore, the TSST is the gold standard approach for psychosocial stress induction in a laboratory setting [All17]. To obtain a control condition, a modified version of the f-TSST was carried out [Wie13]. Depending on the order of conditions, the f-TSST was performed either the day before or the day after the TSST.

4.2.1 Trier Social Stress Test (TSST)

The TSST protocol can be divided into three main parts, each lasting 5 minutes. The first part is the preparation phase, in which the participant was asked by the study leader to take notes about their personality and to fill out a questionnaire. After the preparation phase, the subject was interviewed by a panel of two persons, female and male, wearing white lab coats. The panel was trained not to show any emotions and to communicate with the participant only in pre-defined phrases. Furthermore, the participant was limited to talk about his personality and was asked to maintain constant eye contact. In addition, communication was only allowed with the panel member of the opposite sex. In the last part of the TSST, the participant was asked to subtract 17 from 2043 repeatedly and move on as quickly and accurately as possible until failure. When an error occurred, the participant was informed by the opposite-sex panel member and advised to start again at 2043. To ensure that the recording from the sensors is as free of artifacts as possible, several pauses were inserted into the TSST protocol, during which the participant was asked not to move and to remain silent. The timeline of the TSST is summarised in Figure 4.1.

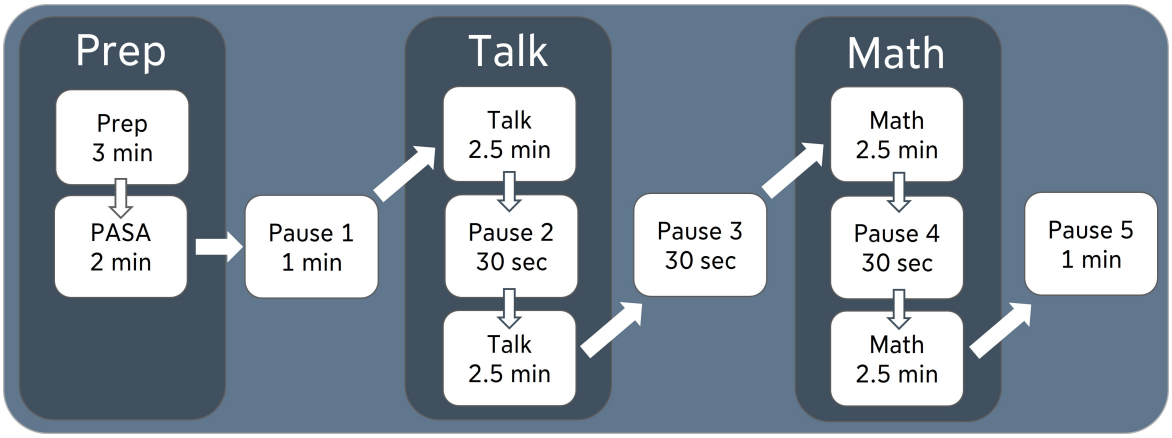

Figure 4.1: Timeline of the (f-)TSST

4.2.2 Friendly Trier Social Stress Test(f-TSST)

The temporal structure of the f-TSST was the same as in the TSST (see Figure 4.1). The difference between the f-TSST and the TSST was the objective appearance of the two-person panel, as they changed into casual clothes. Furthermore, both panel members were allowed to communicate with the participant and were encouraged to respond positively to the subject. The mental arithmetic task was also simplified since the subjects had to alternate adding ten and twenty. When an error occurred, the panel politely informed the participant and allowed them to continue calculating at the same point. In general, the task of the panel was to show interest in the participant's presentation, to be friendly, and to avoid unpleasant situations without going beyond the time frame of the study protocol.

4.3 Measurements

4.3.1 Electrocardiography (ECG)

The ECG allows fast and noninvasive measurement of the electrical activity of the heart with the help of electrodes, placed on the surface of the skin [Hla05; Raf21]. The results of the measurement are presented in the form of a characteristic waveform, showing the variation in the measured voltage [Hla05; AL-15]. In order to receive the electrical activity of the heart from multiple directions, the electrodes can be placed in different positions on the human body [AL-15]. In clinical practice, twelve different electrode configurations are typically used, which are also called leads. This provides spatial information about the electrical activity of the heart [Sam15]. The ECG leads can be divided into two main groups. The so-called limb leads, which consist of three bipolar and three unipolar leads [AL-15], allow the electrical activity of the heart to be displayed from a frontal perspective [Sam15]. The remaining six electrode configurations are the so-called precordial or chest leads [AL-15], which provide information on the heart's electrical activity in the transverse plane [Sam15].

Depending on the chosen lead configuration, the ECG produces different characteristic waveforms [AL-15]. The significant valleys and peaks in the obtained waveform can be divided into six parts: the P, Q, R, S, T, and U wave [AL-15]. For PEP computation, the Q-wave and the R-peak are highly relevant. Both events are a part of the QRS complex, that accounts for the greatest portion of the amplitude in the ECG waveform [McS03]. The Q-wave onset is the starting point of the QRS complex and corresponds to the start of ventricular depolarization [Hla05]. The R-peak is the most prominent point in the ECG waveform and therefore most reliable to detect [See16]. An overview of the ECG waveform with its most prominent events is provided in Figure 4.2.

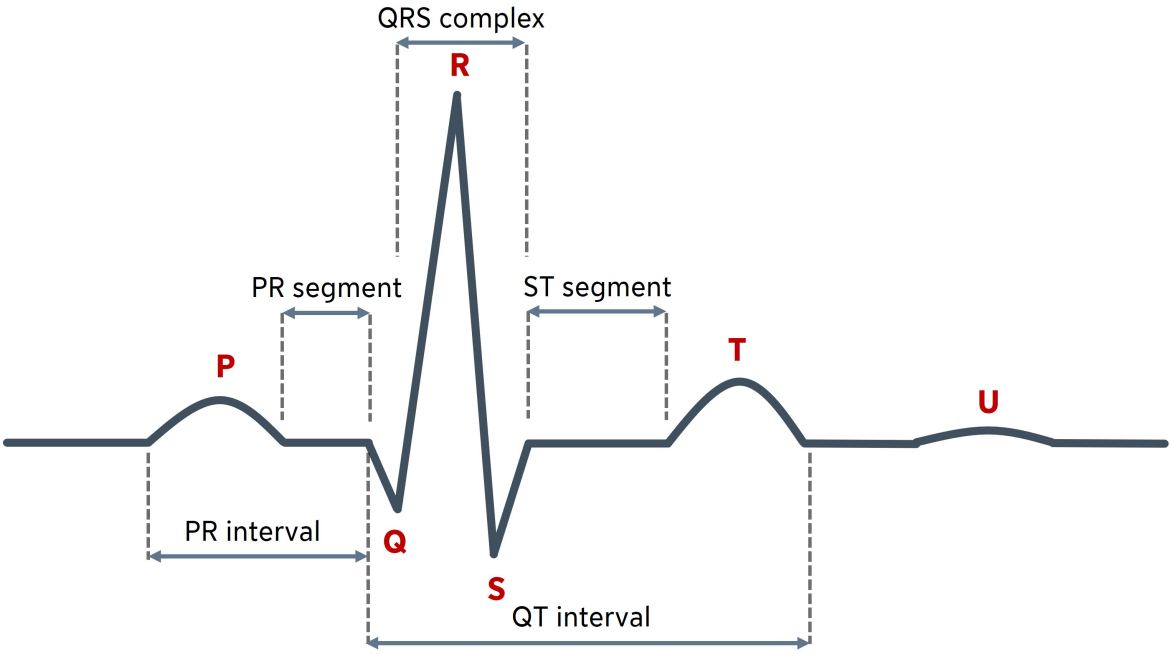

Figure 4.2: Overview of the significant events in the ECG waveform.

Since the usage of the Q-wave onset for PEP computation is questionable [See16], reliable detection of the R-peak is of high importance. To do so, the lead II configuration was used in this study [She90]. Accordingly, one electrode was placed on the right clavicle and one electrode on each of the left and right lowest ribs of the participant. Data were acquired using the Biopac MP160 system and the AcqKnowledge software package [Bio23]. The sampling rate was set to 1000 Hz.

4.3.2 Impedance cardiography (ICG)

PEP is the summation of all electrical and mechanical processes prior to the ejection of blood from the ventricle [New79]. However, the ECG provides information about the electrical activity of the heart, but not about the mechanical activity [Nag89]. To obtain the missing information the ICG can be used to measure systolic time intervals, including PEP [She90]. By applying a high-frequency alternating current to the thorax, a characteristic waveform is created in the first derivative of the ICG signal, which is influenced by the cardiac cycle [Lab70]. The measured impedance changes of the thorax are therefore caused by volumetric changes [Lab70; She90].

The measuring principle of the ICG is based on Ohm's law [She90; Man18].

$$V = Z * I$$

A constant alternating current field I directed along the thorax, is applied [She90]. Furthermore, electrodes measuring the voltage difference V of the thorax are attached [Man18]. Therefore, a change in impedance Z can be measured as a function of blood flow since blood is conductive [She90; Man18]. This is due to the proportionality between the measured voltage and the impedance of the thorax [Cyb12]. Thus, impedance changes in the ICG reflect blood flow in the aorta since it is equally directed regarding the current field [She90].

A frequently used method to measure the ICG is based on the use of 8 spot electrodes [She90]. Therefore, four electrodes are placed on the neck and four electrodes are placed on the lower part of the chest. Accordingly, one of the voltage electrodes is placed on each side just above the clavicle. In addition, one voltage electrode is placed laterally on each side at the height of the xiphoid process. The current electrodes are placed in parallel on the neck 5 cm above and on the chest 5 cm below the voltage electrodes [She90]. This electrode placement was also used in this study. As with the ECG, the Biopac MP160 system and the AcqKnowledge software package were used for data acquisition [Bio23]. An overview of the electrode placement is given in Figure 4.3.

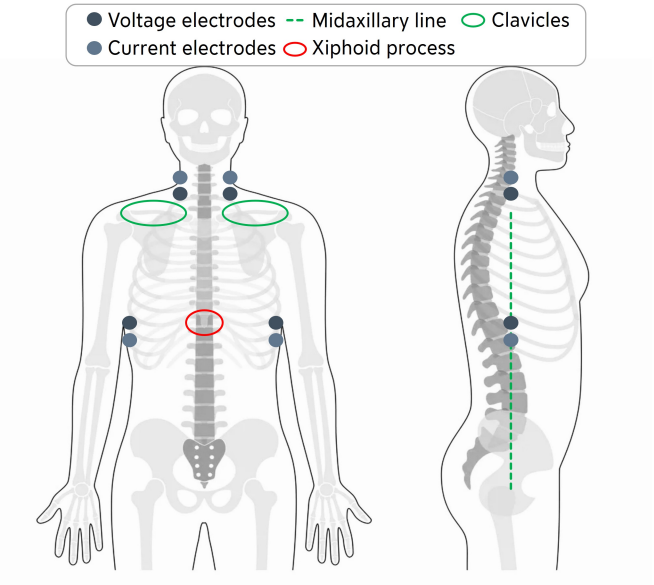

Figure 4.3: Overview of the electrode placement for the ICG measurement.

Just as with the ECG, the ICG also produces a characteristic waveform [Lab70]. The relevant points for PEP computation are the A-, B-, and C-points respectively. The A-point, whose typical shape is caused by the contraction of the atrium, represents the beginning of electromechanical systole [Man18]. This point corresponds to the most significant minimum prior to the C-point [For18]. The start of blood ejection from the left ventricle, which indicates the end of PEP corresponds to the B-point [She90]. At this point, the dZ/dt signal begins to rise to its maximum [She90]. After the aortic valve is opened and the maximum

blood flow through the aorta is reached, the C-point occurs [She90]. This point reflects ventricular contraction and represents the maximum in the dZ/dt waveform [She90; Man18]. Although there are characteristic points in the waveform, their appearance can differ. In particular, the morphology of the B-point can vary greatly between individuals and even within individuals [She90; For18]. Some common B-point morphologies, as well as the A- and C-points of the dZ/dt signal, are therefore shown in Figure 4.4.

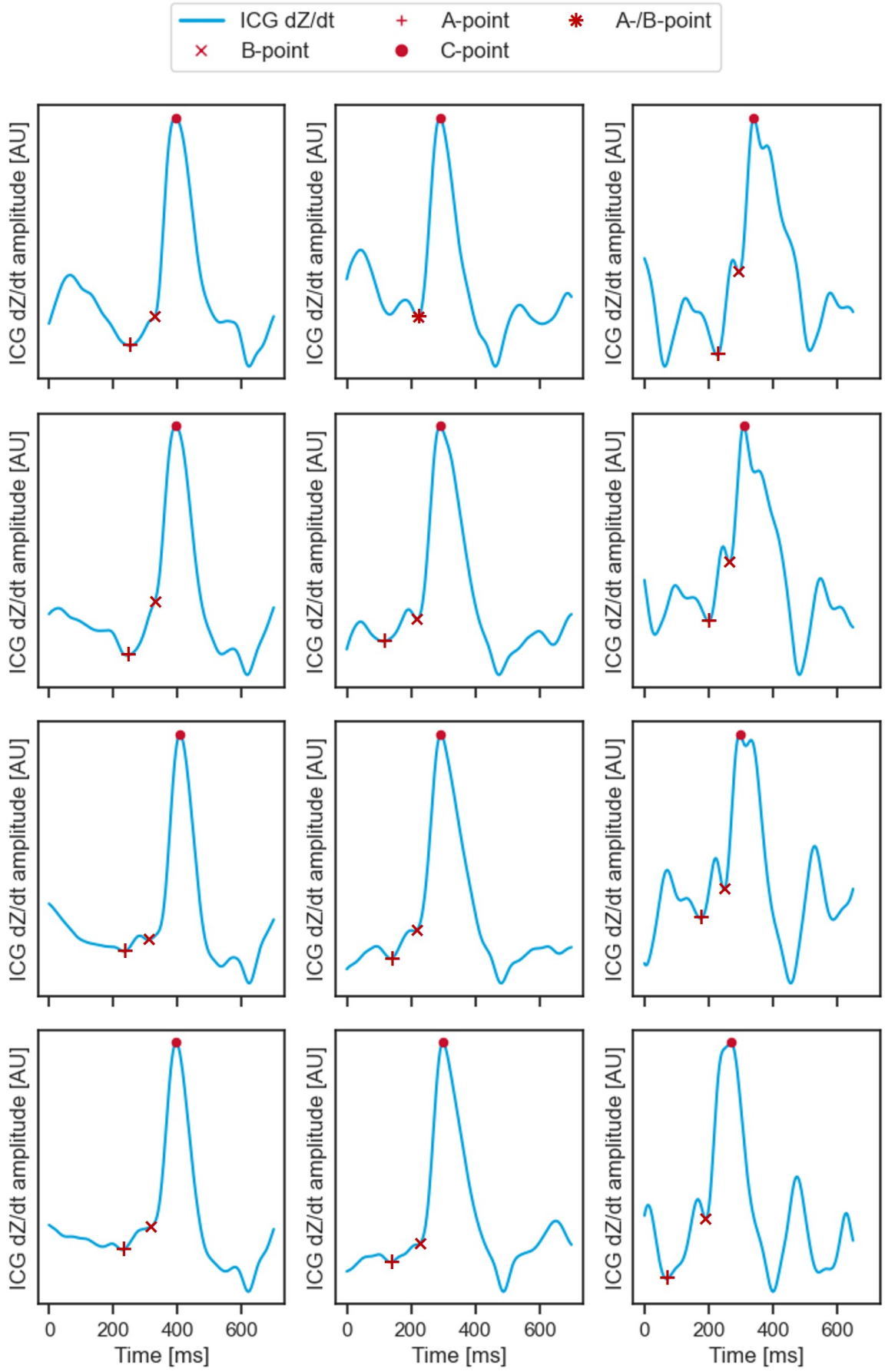

Figure 4.4: Overview of different B-point morphologies within subjects (rows) and between subjects (columns).

4.4 Reference Data

To obtain the accuracy of the implemented algorithms, a reference dataset was generated. The recorded ICG and ECG data of 15 participants was used to label subsections from each of the following phases: Pause 1, Prep, Talk, Math, and Pause 5. Ten seconds in each of the Pause 1 and Pause 5 phases were labeled. In the remaining phases, 30 seconds were labeled. The Talk and Math phases also include a 30 second speaking break, which was not labeled separately, but was combined with the phases just mentioned, to form an overall phase. In order to obtain a variation in the manually labeled subsections, the starting points were chosen randomly within the borders of the corresponding phases. In total 5086 cardiac cycles were labeled using the *MaD GUI* [Oll22]. This is a Python package that allows multiple signals to be displayed simultaneously, to load pre-annotated data, and to generate individual labels.

Q-wave onset

In this study, not every participant showed a clearly recognizable Q-wave. Consequently, it was impossible to mark the Q-wave onset without variance between study participants. This observation is consistent with experience in related work, where the visibility of the Q-wave is known to be an issue [She90]. Following the results of a study conducted by Berntson et al., the detection of the R-onset is the more reliable approach to detect the start of PEP [Ber04]. The R-onset is described as the sharp rise in slope before the R-peak. In the presence of a Q-wave, this point coincides with the tip of the Q-wave [See16]. After trying different ECG cleaning approaches, it was found that using the *biosppy* method of the *neurokit2* package reveals the clearest Q-waves. To pre-label the data, the ECG delineate method of the *neurokit2* python package was used, which is capable of detecting the components of the QRS complex [Mak21]. To avoid the occurrence of errors and to ensure the reliable and consistent detection of the R-onset, the pre-labeled data was visually inspected afterward.

B-Point

The B-point can occur in various morphologies, complicating pinpointing the correct B-point [She90; For18]. To cover this variety and to mark the B-points as accurately as possible, a visual decision tree published by Árbol et al. was used to label the B-points in this study [Árb17]. Additionally, the examples of hard-to-detect B-points proposed by Forouzanfar et al. were used [For18]. To further simplify the labeling process, the ECG and ICG signals were loaded into the *MaD Gui* simultaneously. Thus, the R-peak could be used as an additional feature to narrow down the search interval for B-point detection, which is done in the same way in related work [For18].

When reliable extraction of the R-onset or the B-point was not possible due to artifacts or waveforms, that did not match any description, these points were marked as artifacts. This was needed to prevent falsification of the reference data and thus false results when comparing the algorithms.

4.5 Automatic Event Detection

4.5.1 Preprocessing

In order to detect the events necessary for PEP computation, interfering factors had to be removed from the ECG and ICG data. The ECG is often influenced by baseline drifts, electromyogram noise, and power-line interference [Chr04]. To remove these distorting effects, the *biosppy* method from the *neurokit2* was applied to clean the ECG [Mak21]. In this method a finite impulse response (FIR) bandpass filter with a filter order of $0.3 * sampling\_rate$ was used. The lower and higher cutoff frequencies were set to 3 Hz and 45 Hz, respectively [Car15]. The ICG signal is also often disturbed by high-frequency noise, baseline drifts, and artifacts [For18]. To counteract this, a 4-th order Butterworth bandpass filter with cutoff frequencies of 0.5 Hz and 25 Hz was applied in forward and backward directions in accordance with related work [For19].

Furthermore, in order to enable a beat-to-beat PEP computation, a heartbeat segmentation was carried out. Sternemann developed a method using the *neurokit2* Python package to perform the heartbeat segmentation [Ste23; Mak21]. This results in the position of the R-peak and the start and end points of the corresponding heartbeat. To determine the heartbeat's start and end points, the RR intervals with the preceding and following R-peaks were calculated. Therefore, the current heartbeat's start point was 65% of the distance from the previous R-peak, and the end point was set to 65% of the following RR interval after the current R-peak [Ste23].

4.5.2 Q-wave onset

Various methods for calculating the Q-wave onset have been discussed in related work. In this thesis, three typically used detection algorithms were implemented. One uses the R-peak, in another approach a constant time interval is subtracted from the R-peak, and the last method uses the Q-peak to estimate the Q-wave onset. In the following section, the implementation of the algorithms is explained in detail.

R-Peak

Detecting the R-peak is not usually a major challenge, as it is the most significant point in the ECG waveform [See16]. This is why other work has suggested the R-peak as the starting point of PEP since it almost eliminates the variance between subjects [See16]. As mentioned above, the R-peaks were already calculated for heartbeat segmentation, since it was only necessary to read out the heartbeat data-frame, to obtain the R-peaks per heartbeat.

R-Peak - constant QR interval

The second approach is also based on the detection of the R-peak, which is extracted in the same way as described in the previous section. In addition, 40 ms were subtracted from each R-peak location to estimate the time of the Q-wave onset. The duration of 40 ms was chosen in accordance with the results of previous investigations [Lie13]. Accordingly, using a constant time interval is valid due to the low variability of the QR interval, even under different physical and psychological conditions [Kro17; Pil23]. The theoretical basis of the algorithm is visualized in Figure 4.5.

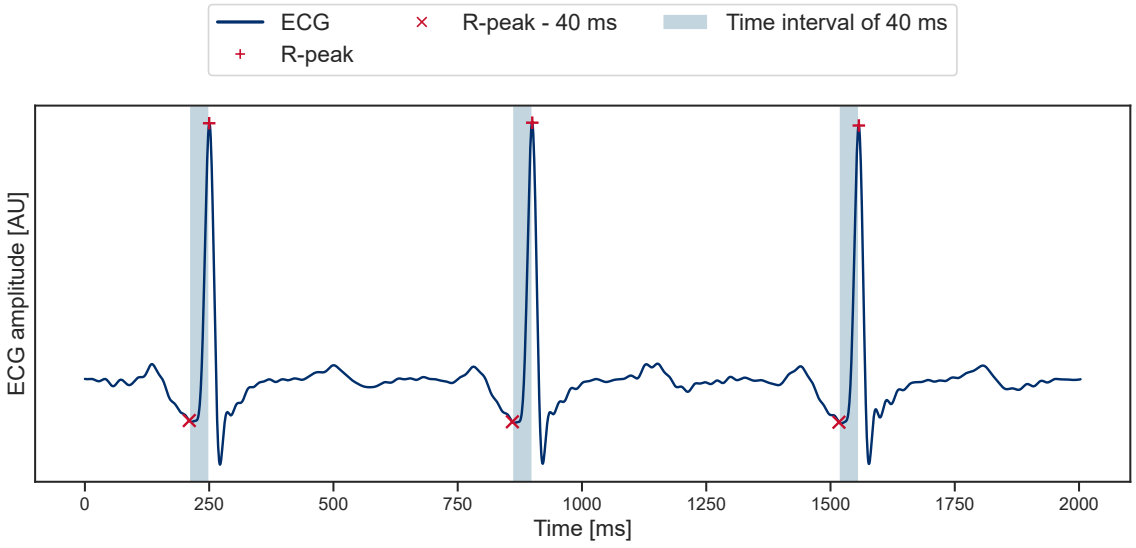

Figure 4.5: Estimation of the Q-onset by subtracting 40 ms from the R-peak location.

Q-Peak

The last method for estimating the Q-wave onset is based on the detection of the Q-peak. Bernston et al. recommend using the R-onset, which corresponds to the Q-peak in the presence of a Q-wave, for detecting the Q-wave onset since this method works independently of the

occurrence of a Q-wave and thus reduces the risk of between subject variance [Ber04]. To obtain the Q-peak a method implemented by Sternemann was used in this work [Ste23]. Thereby, the Q-peak location was extracted by the ECG delineate method from the *neurokit2* library, which performs a discrete wavelet transform (DWT) to detect the significant events in the ECG waveform [Mak21].

4.5.3 B-Point

For B-point detection, four algorithms were used in this work. In addition to plain B-point extraction, outlier correction algorithms were also implemented, which will be introduced in more detail later. In all B-point extraction algorithms, a parameter that can be used to specify whether or not outliers are to be corrected afterward was implemented. This parameter had an influence in the cases where no B-points could be detected. In addition, the C-point was passed to each of the detection algorithms, as it serves as the right boundary for B-point determination. The procedure to extract the C-point is therefore described first.

C-Point

As many B-point detection algorithms are based on the extracted C-points, their detection is crucial to avoid falsification of the obtained B-points. The C-point, which represents the time of maximal blood flow through the aorta, corresponds to the global maximum of the dZ/dt signal for each heartbeat [She90]. This allows easy automatic detection in most cases. However, Sternemann observed, that the detection of the C-point in a data set with physiologically similar expected responses to this study, was prone to error [Ste23]. Therefore, an adapted C-Point extraction algorithm was developed based on a peak detection method of the *scipy* library [Vir20]. When multiple peaks were found in one heartbeat, the average distance of the three previous C-points to the corresponding R-peaks was calculated. Afterward, the peak with the smallest deviation from the average distance was selected as the C-point [Ste23].

Reversal point of the dZ^2/dt^2 signal

The first B-Point detection algorithm is based on pinpointing the reversal point in the $\boldsymbol{dZ^2/dt^2}$ signal [Deb93]. This point corresponds to an inflection point in the dZ/dt signal, which is one possible B-point morphology [Árb17]. In order to find this point, local minima in the $\boldsymbol{dZ^2/dt^2}$ signal between the R-peak and the C-point were extracted. When multiple minima occurred, the one closest to the C-point was chosen. When outlier correction was performed, the B-point was set to the beginning of the search interval, which corresponded to the R-peak, in cases

where no local minimum could be detected in the dZ^2/dt^2 signal. The relationship between the selected local minima in the dZ^2/dt^2 signal and the detected B-points is illustrated in Figure 4.6.

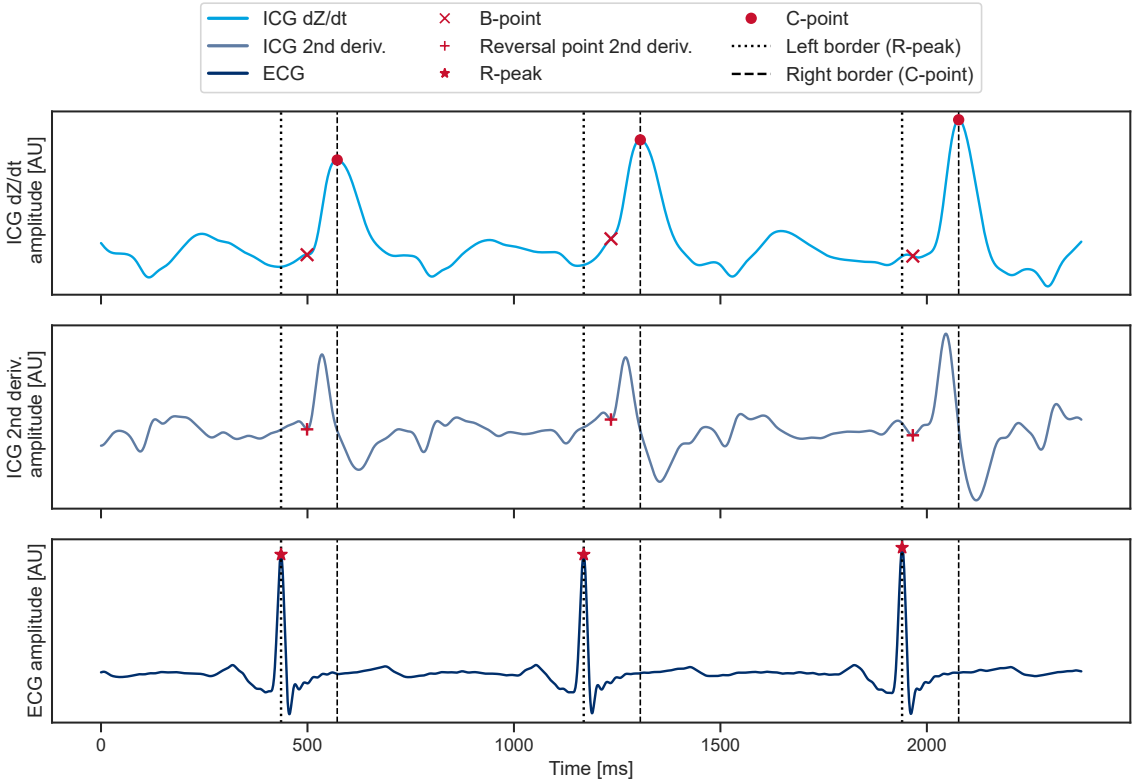

Figure 4.6: B-point detection based on the reversal point of the dZ^2/dt^2 signal.

Maximum of the third derivative of the cardiac impedance (dZ^3/dt^3) signal

Another B-point detection algorithm, based on the calculation of higher derivatives, was developed by Arbol et al.. Thereby, the local maximum in the dZ^3/dt^3 signal is detected since this point corresponds to the point with the greatest change in slope in the dZ/dt signal, which is another possible B-point morphology. To ensure the most accurate detection and robustness to interfering factors, the search area for the local maximum is limited to a certain time interval before the C-point [Árb17]. In this work, it was possible to use an implementation of this algorithm by Sternemann. Following the literature, the time interval was set to 150 ms in this work [Ste23]. An illustration of the described algorithm is provided in Figure 4.7.

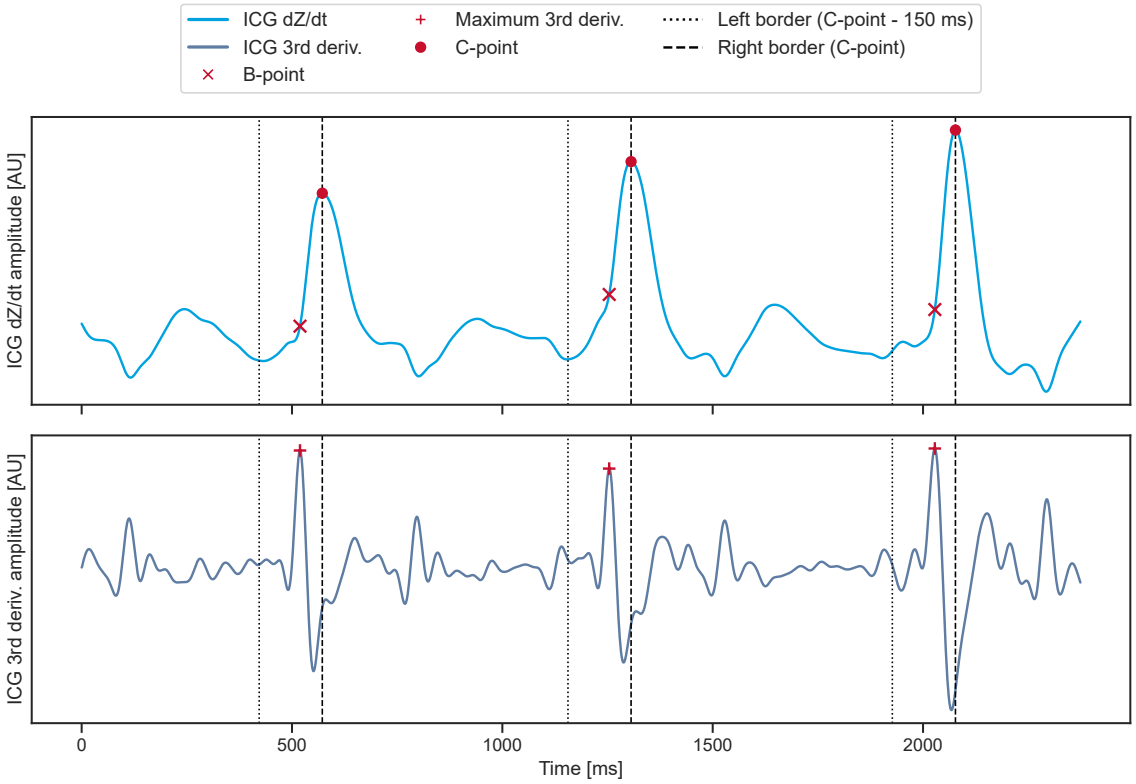

Figure 4.7: B-point detection based on the maximum in the dZ^3/dt^3 signal.

Maximal Distance from a straight line to the dZ/dt signal

Detecting significant events in the dZ^2/dt^2 or dZ^3/dt^3 signal is the basis of many frequently used B-point detection algorithms [Árb17]. However, Drost et al. developed a method to detect B-points, based on the dZ/dt signal only. Therefore, a straight line was drawn from the C-point to the point that occurred 150 ms before the C-point in the dZ/dt signal. Following, the point, which showed the maximal vertical distance between the straight line and the dZ/dt signal was chosen as the B-point [Dro22]. The principle of the algorithm is illustrated in Figure 4.8.

Algorithm based on multiple decision rules

Finally, a novel automatic algorithm, developed by Forouzanfar et al., was implemented. In addition, to plain B-point detection, an outlier correction step using an autoregressive model was performed [For18]. Since the outlier correction algorithm was also applied to the other B-point detection algorithms, it is explained in section 4.5.4 and section 4.5.5. Unlike other commonly used algorithms, the proposed approach is not based on a fixed rule [For18]. Instead, Forouzanfar et al. used several steps to limit the search area and multiple decision

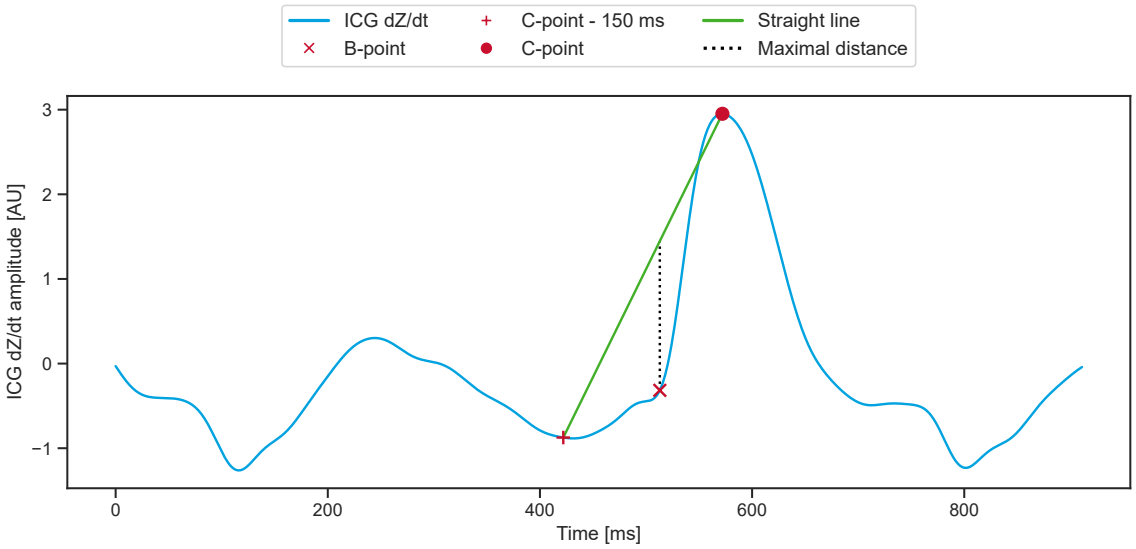

Figure 4.8: Calculation of the maximal vertical distance between the dZ/dt signal and a straight line between the C-point and the point 150 ms prior to the C-point to estimate the B-point location.

rules were introduced to locate the correct B-point [For18]. To reduce the search interval, the A-point, which represents the most significant minimum before the C-point, was first detected within one-third of the beat-to-beat interval, prior to the C-point [For18]. In this work, the beat-to-beat interval was defined as the distance between the current C-point and the previous C-point. To further reduce the search range, all monotonically increasing segments in the previously extracted interval were detected. Unlike Forouzanfar et al. explanation, the segment starting below half the C-point amplitude and ending above two-thirds of the C-point amplitude was selected [For18]. This change was made since otherwise no monotonic segment could be detected in cases without inflection or reversal point between the A- and C-point. According to related work, the C-point amplitude was therefore defined as the distance from the zero line at the location of the C-point [She90]. To finally locate the B-point, the first third of the most significant monotonic segment was searched for zero crossings in the $\boldsymbol{dZ^3/dt^3}$ signal and for local maxima in the $\boldsymbol{dZ^2/dt^2}$ signal. The zero crossings, that correspond to a too-large slope in the dZ/dt signal have been neglected. Therefore, a threshold was set to $10 * H/f_s$, and zero crossings with a higher $\boldsymbol{dZ^2/dt^2}$ value were omitted. In order to use only the significant local maxima, all those whose values of the $\boldsymbol{dZ^3/dt^3}$ signal were less than $4 * H/f_s$, have been abandoned [For18]. The height H has been defined as the difference in amplitude between the A-point and the C-point and f_s corresponds to the sampling rate [For18]. As a last step, the zero crossing, or the local maximum of the $\boldsymbol{dZ^3/dt^3}$ with the smallest distance to the C-point, was defined as the B-point. The first point

of the detected monotonically increasing segment was chosen if neither of the two points existed [For18]. When outlier correction was performed, the B-point was set to the R-peak in cases where no monotonic segment could be found to achieve beat-to-beat PEP computation.

4.5.4 B-Point Outlier Detection

To detect those points that were too far or too close to their neighbors in either time or amplitude, B-point outlier detection was performed, based on the work of Forouzanfar et al. [For18]. According to this, the B-point time data had to be stationarized before the outliers could be detected. To obtain the stationarized data, the B-point time data baseline was calculated and subtracted from the original B-point time data [For18]. To compute the B-point time data baseline, a 4-th order Butterworth low-pass filter with a cutoff frequency of 0.1 Hz was applied to the B-Point time data, in forward and backward direction [For18]. Due to the lack of description of the procedure, it was assumed that the sampling rate of the B-point time data is 1 Hz, which means that the B-points are equally sampled. Furthermore, the B-point time data was obtained by calculating the difference between the C-points and the corresponding B-points. To finally detect the outliers, the median and the median absolute deviation of the stationarized B-point time data were calculated. Subsequently, the B-points that were three times as far away from the median as the median absolute deviation were marked as outliers [For18].

4.5.5 B-Point Outlier Correction

After the outliers were detected, they still had to be corrected. Therefore, two outlier correction methods were implemented in this work. The first approach belongs to the outlier detection algorithm published by Forouzanfar et al. and is based on an autoregressive model and the other method uses interpolation to correct the obtained outliers.

Autoregressive Model

Autoregressive models are often used to estimate the future course of time series data. Applications include predicting economic dynamics or the evolution of the COVID-19 pandemic, to name two examples [Lüt05; Mal20]. However, Forouzanfar et al. used this method to correct the B-point outliers by performing autoregressive model prediction in forward and backward direction [For18]. The corrected B-points were then calculated as the average of the forward and backward predictions [For18]. An *Autoregressive Integrated Moving Average (ARIMA)* model from the *statsmodels* library was used to implement the autoregressive model in this work [Sea10]. To stay in line with Forouzanfar et al. the integration *(I)* and moving average

(MA) components were set to zero, so that only the autoregressive model was obtained. To calculate the parameters and the order of the forward and backward autoregressive models, Burg's method and minimization of the Akaike information criterion (AIC) were used respectively [Aka69; Kay88; For18]. Finally, the baseline was added back to the B-point time data [For18]. Then outliers were searched again, and if any were found, the outlier correction procedure was repeated. The process was completed when no more outliers were detected. [For18].

Linear Interpolation

As an alternative approach to correct the B-point outliers, linear interpolation was chosen for its simplicity and efficiency [Lep17; Kul21]. Using this technique, a straight line is fitted between the two neighboring values to estimate the outlier [Lep17]. In this study, linear interpolation was performed using the *interpolate* method of the *pandas* library [tea20].

Chapter 5

Results & Discussion

To investigate whether PEP is capable of reflecting changes in the individual's stress level induced through the (f-)TSST and to compare the performance of several event detection pipelines for automatic PEP computation, the Q-onsets and B-points of 5086 cardiac cycles were manually labeled in this work. This chapter provides an overview of the obtained results and discusses them with respect to related work.

5.1 Effects of the TSST on PEP duration

In order to determine whether PEP is an appropriate marker to reflect changes in the individual's stress level, the variation of the manually labeled reference data through the (f-)TSST timeline is investigated in the following section. In total 5086 cardiac cycles were manually labeled in this work. The mean and standard deviation of PEP were 88.49 ms and 25.10 ms, respectively. Minimum and maximum values of the manually labeled reference data were 26 ms and 266 ms. In addition, the mean and standard deviation of the f-TSST and TSST were calculated separately. For the f-TSST, a mean of 92.62 ms with a standard deviation of 25.39 ms was observed for 2393 labeled cardiac cycles. The mean PEP in the TSST amounted to 84.81 ms with a standard deviation of 24.25 ms. This was obtained from the remaining 2693 labeled cardiac cycles. All of the mean PEP values are within the physiologically normal range, which includes a PEP duration between 70 ms and 175 ms [Árb17]. An overview of the received PEP parameters is given in Table 5.1. Furthermore, the obtained differences can also be seen in Figure 5.1 since there is a visible difference between the f-TSST and TSST condition.

In addition, the mean and standard deviation of the phases of the (f-)TSST were calculated separately. Both, TSST and f-TSST, showed a decrease of mean PEP values between Prep and Pause 1. Minimum PEP durations of 77.44 ms for the TSST and 78.66 ms for the f-TSST

Table 5.1: Obtained parameters of the manually labeled reference PEP data.

	Cardiac cycles	PEP Mean ± SD	PEP min	PEP max
Total	5086	88.49 ± 25.10	26.00	266.00
f-TSST	2393	92.62 ± 25.39	26.00	180.00
TSST	2693	84.81 ± 24.25	27.00	266.00

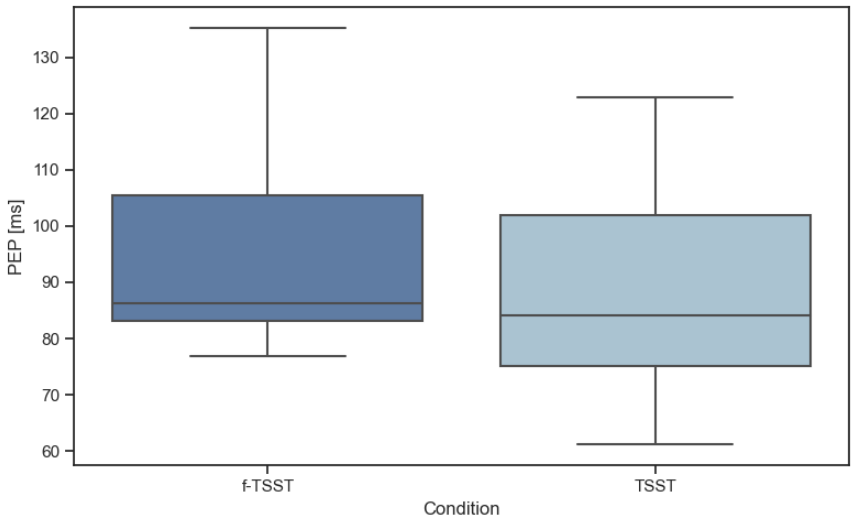

Figure 5.1: Overview of the reference PEP values grouped by condition.

were obtained in Pause 1. In the following, PEP increased in both conditions until they reached their maximum values in Pause 5. The maximum values were 99.19 ms in the TSST and 111.30 ms in the f-TSST. Accordingly, the mean PEP values, even when broken down to phases, were within the physiological limits [Árb17]. Detailed information of the obtained PEP parameters is provided in Table 5.2. The observed trend of the mean PEP is illustrated in Figure 5.2.

Discussion

The clearly discernible 8.43% drop in mean PEP duration from the f-TSST to the TSST suggests, that PEP is capable of reflecting the difference in the participant's stress levels, caused by psychosocial stress induction. The difference between the f-TSST and TSST could also be obtained on the phase level, except for Pause 1. In this phase, mean PEP duration is only slightly different between the f-TSST and TSST. A possible explanation for this observation is that during Pause 1 the participants were unaware of the upcoming stress test procedure. In addition, they have either no knowledge of the (f-)TSST procedure when it was the first day, or possibly negative experiences if they performed the TSST on the previous day. The sharp increase of PEP in Pause 5 suggests that participants relax in this phase. This

Table 5.2: Overview of PEP per phases and condition; Mean ± SD

Condition	Phase	Cardiac cycles	PEP Mean ± SD
f-TSST	Prep	621	87.94 ± 24.43
	Pause 1	225	78.66 ± 20.49
	Talk	712	93.66 ± 24.73
	Math	635	95.11 ± 25.78
	Pause 5	200	111.30 ± 21.31
TSST	Prep	692	81.77 ± 21.45
	Pause 1	231	77.44 ± 24.42
	Talk	787	85.68 ± 28.28
	Math	769	84.86 ± 20.59
	Pause 5	214	99.19 ± 22.72

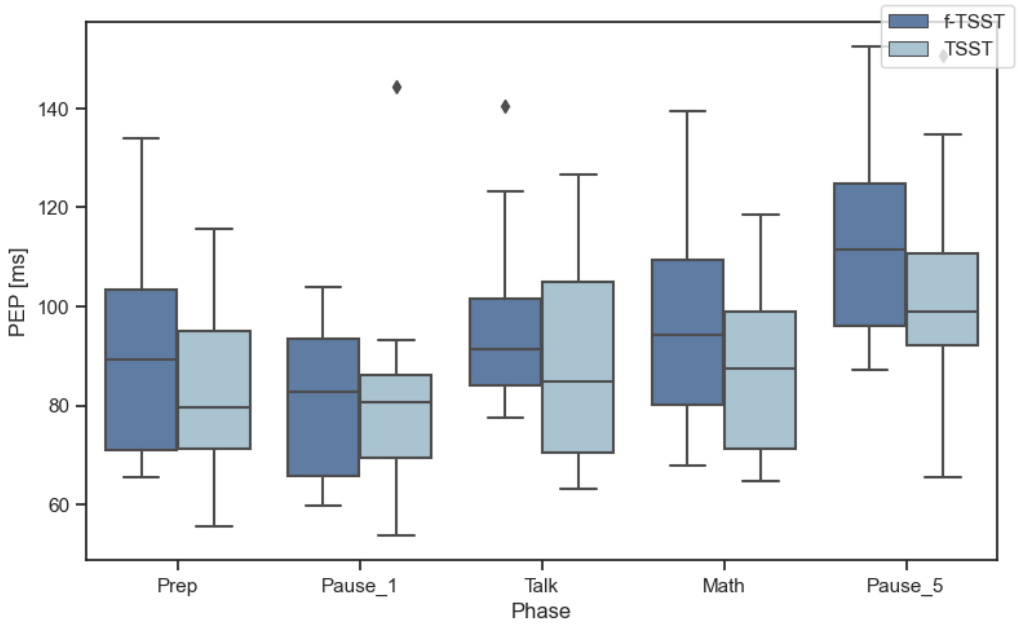

Figure 5.2: Overview of the reference PEP values grouped by phases.

is because they are told beforehand that the test is about to end after this break. The large standard deviation of over 20 ms observed in both conditions and in all phases is an indicator of a large variance in the response of the individuals to the psychosocial stress induction. The results of this investigation reveal that PEP is capable of reflecting changes in the human stress level not only between the f-TSST and TSST but also on the phase level.

5.2 PEP Estimation

Furthermore, the performance of the implemented PEP computation pipelines was investigated. In total, three Q-onset detection, four B-point detection, and two outlier correction algorithms were implemented in this work. This resulted in 36 possible event detection pipelines. An overview of how the PEP computation pipelines were assembled by the individual components is illustrated in Table 5.3.

Table 5.3: Overview of the individual algorithms used to assemble the 36 PEP computation pipelines.

Q-wave onset	B-point	Outlier correction
R-peak	Reversal point of the $\boldsymbol{dZ^2/dt^2}$ signal	Without outlier correction
R-peak - 40 ms	Maximum of the $\boldsymbol{dZ^3/dt^3}$ signal	Linear interpolation
Q-peak	Maximal vertical distance from the dZ/dt signal to a straight line between the C-point and the point 150 ms prior to the C-Point Algorithm based on multiple decision rules and thresholds	Autoregressive model

To compare the performance of the obtained PEP computation pipelines, the MAE, mean error (ME), and the median (Md) of each pipeline were calculated against the manually labeled reference data. The algorithm combination of a constant time interval of 40 ms, the reversal point of the $\boldsymbol{dZ^2/dt^2}$ signal and no outlier correction showed the best performance. The MAE was 14.58 ms with a standard deviation (SD) of 19.30 ms respectively. However, PEP values were only obtained for 4696 out of 5086 cardiac cycles. Since the aim of this Bachelor's thesis was the beat-to-beat PEP computation, this pipeline cannot be used for this purpose. The PEP computation pipeline, which showed the second-best performance was the before mentioned approach with an autoregressive model for outlier correction. The MAE of 15.31 ms with a SD of 19.20 ms showed the minimal difference to the best approach. Regarding the detection rate, the use of the autoregressive model resulted in a strong improvement in performance. Accordingly, PEP values were obtained in 5081 out of 5086 cardiac cycles. This corresponds to an error rate of 0.00098%. A higher detection rate could not be reached with other PEP computation pipelines.

Another interesting observation is the decent performance of the PEP computation pipeline based on the R-peak, the third derivative, and outlier correction with interpolation. The MAE was 16.30 ms with a SD of 12.79 ms and a detection rate of 5080 out of 5086 cardiac cycles.

This is surprising, since most algorithms that use the R-peak but not the third derivative showed poor performance. The result suggests that the method based on the third derivative compensates for the late occurrence of the R-peak compared to the other algorithms. This theory is supported by the poor performance of the third derivative method in combination with the Q-peak method and the approach subtracting 40 ms from the R-peak. To verify the assumption, that an overestimation of the B-point location through the third derivative method compensates for the late occurrence of the R-peak further investigations are carried out in section 5.2.2. The PEP computation pipelines using the B-point detection method, based on multiple decision rules and outlier correction with an autoregressive model, which showed superior performance in prior investigations did not perform well in this work [For18]. A MAE of 19.51 ms and a SD of 20.13 ms are supporting this observation. Detailed information about the performance of all possible PEP computation pipelines is provided in Table 5.4. Looking at the influence of the outlier correction methods on the MAE of PEP, variations in the performance can be observed. Even between the same B-point detection methods, the outlier correction may lead to either an improvement or a deterioration of the mean absolute error depending on the choice of the R-onset detection method. This leads to the assumption that the performance of the entire PEP computation pipeline and the choice of the B-point detection algorithm is strongly dependent on whether the automatic R-onset detection method under or over-estimates its occurrence. To verify this assumption, further investigations were carried out regarding the accuracy of the algorithms for calculating the start and end points of PEP.

Table 5.4: Overview of the performance of all automatic PEP computation pipelines. The table contains information about the amount of detected PEP values, ME, MAE, and Md of each PEP computation pipeline.

Q-onset	B-point	Correction	Cardiac Cycles	MAE ± SD	ME ± SD	Md
Q-peak	Multiple conditions	—	5006	24.00 ± 26.52	-19.27 ± 30.13	-8.0
		Autoregression	5072	21.93 ± 23.11	-15.55 ± 27.81	-7.0
		Interpolation	5072	21.43 ± 22.90	-14.50 ± 27.81	-7.0
	Second derivative	—	4696	17.32 ± 17.60	-2.68 ± 24.55	-9.0
		Autoregression	5081	17.17 ± 17.50	-0.25 ± 24.52	-7.0
		Interpolation	5081	17.80 ± 18.18	2.29 ± 25.34	-6.0
	Straight line	—	5081	17.55 ± 16.75	12.20 ± 20.96	11.0
		Autoregression	5081	17.94 ± 16.23	15.42 ± 18.63	12.0
		Interpolation	5081	18.36 ± 16.65	16.35 ± 18.63	12.0
	Third derivative	—	5080	26.22 ± 19.56	21.43 ± 24.72	18.0
		Autoregression	5080	27.99 ± 19.27	26.99 ± 20.65	23.0
		Interpolation	5080	28.83 ± 19.60	27.98 ± 20.79	24.0
R-peak	Multiple conditions	—	5006	53.62 ± 28.40	-53.46 ± 28.71	-44.0
		Autoregression	5072	50.23 ± 25.34	-49.73 ± 26.29	-43.0
		Interpolation	5072	49.34 ± 25.09	-48.68 ± 26.35	-42.0
	Second derivative	—	4696	41.25 ± 15.34	-36.90 ± 23.99	-42.0
		Autoregression	5081	38.70 ± 16.12	-34.43 ± 23.92	-39.0
		Interpolation	5081	36.93 ± 16.48	-31.89 ± 24.87	-38.0
	Straight line	—	5081	23.63 ± 17.86	-21.97 ± 19.87	-21.0
		Autoregression	5081	21.44 ± 14.28	-18.75 ± 17.66	-20.0
		Interpolation	5081	21.01 ± 13.79	-17.83 ± 17.71	-19.0
	Third derivative	—	5080	19.78 ± 18.34	-12.75 ± 23.77	-14.0
		Autoregression	5080	16.46 ± 12.89	-7.19 ± 19.63	-10.0
		Interpolation	5080	16.30 ± 12.79	-6.20 ± 19.77	-9.0
Time interval	Multiple conditions	—	5006	21.34 ± 23.45	-13.46 ± 28.71	-4.0
		Autoregression	5072	19.51 ± 20.13	-9.73 ± 26.29	-3.0
		Interpolation	5072	19.23 ± 20.00	-8.68 ± 26.35	-2.0
	Second derivative	—	4696	14.58 ± 19.30	3.10 ± 23.99	-2.0
		Autoregression	5081	15.31 ± 19.20	5.57 ± 23.92	1.0
		Interpolation	5081	16.63 ± 20.20	8.11 ± 24.87	2.0
	Straight line	—	5081	22.48 ± 14.65	18.03 ± 19.87	19.0
		Autoregression	5081	23.10 ± 15.16	21.25 ± 17.66	20.0
		Interpolation	5081	23.65 ± 15.67	22.17 ± 17.71	21.0
	Third derivative	—	5080	31.29 ± 18.12	27.25 ± 23.77	26.0
		Autoregression	5080	33.52 ± 18.39	32.80 ± 19.63	30.0
		Interpolation	5080	34.42 ± 18.68	33.80 ± 19.77	31.0

5.2.1 Q-wave onset

In this chapter, the R-onset detection methods were examined in isolation to test their accuracy in extracting the manually labeled reference point and to identify possible trends of under- or over-estimation of this point. Therefore, the MAE, ME, and the Md of each R-onset detection algorithm were calculated with respect to the reference data in line with the previous chapter. Another aim of this section is whether subtracting 40 ms from the R-peak, which was used in related work to estimate the Q-onset [Lie13], is the best approach to estimate the R-onset, which was used as the starting point of PEP in this work [Ber04]. Therefore, the performance when using values between 30 ms and 50 ms were tested. An overview of the obtained results is provided in Table 5.5.

Table 5.5: Overview of the performance of the Q-onset detection methods with regard to the manually labeled reference data.

Algorithm	MAE ± SD	ME ± SD	Md
Q-peak	2.87 ± 7.51	-2.54 ± 7.51	0.0
R-peak	31.63 ± 6.96	31.63 ± 6.96	33.0
R-peak - 30ms	6.10 ± 3.73	1.63 ± 3.73	3.0
R-peak - 32ms	5.71 ± 3.40	-0.37 ± 4.00	1.0
R-peak - 34ms	5.62 ± 4.74	-2.37 ± 4.74	-1.0
R-peak - 36ms	6.07 ± 5.55	-4.37 ± 5.55	-3.0
R-peak - 38ms	7.23 ± 6.07	-6.37 ± 6.07	-5.0
R-peak - 40ms	8.78 ± 6.43	-8.37 ± 6.43	-7.0
R-peak - 42ms	10.59 ± 6.62	-10.37 ± 6.63	-9.0
R-peak - 44ms	12.50 ± 6.73	-12.37 ± 6.73	-11.0
R-peak - 46ms	14.48 ± 6.74	-14.37 ± 6.74	-13.0
R-peak - 48ms	16.46 ± 6.75	-16.37 ± 6.75	-15.0
R-peak - 50ms	18.45 ± 6.76	-18.37 ± 6.76	-17.0

Each R-onset detection method was able to achieve results for all 5086 cardiac cycles. Regarding the MAE, using the Q-peak, to estimate the R-onset showed the least deviation from the reference data. The MAE was 2.87 ms with a SD of 7.51 ms. This observation seems logical, since the R-onset, which is coincident with the Q-peak in the presence of a Q-wave, was labeled as the start point of PEP in this work. This was done, according to the recommendation of Bernston et al. [Ber04]. Furthermore, the same Q-peak detection algorithm used for automatic Q-peak detection was also used for pre-labeling, which reinforces the high agreement. Looking at the residual plot of the Q-peak detection algorithm in Figure 5.3, it is noticeable that most of the points are lying close to the zero line. This indicates that the R-onset was correctly detected by the Q-peak detection algorithm. Hence

no manual correction was necessary afterward. On the other hand, scattering in the negative y-direction can also be observed. To obtain the reference data, a manual correction was necessary in these cases since the Q-peaks occurred too early, which can be seen in the negative mean error of -2.53 ms and the observed trend in the residual plot.

The use of the R-peak to estimate the R-onset leads to the largest mean absolute error of 31.630 ms. This is consistent with the results of the PEP analysis, where most of the PEP computation pipelines using the R-peak for R-onset estimation showed poor performance. The reason for this observation is a systematic overestimation of the R-onset location through the R-peak approach. This can either be seen in the positive mean error of 31.63 ms and in the positive offset in the residual plot (Figure 5.3).

Investigations regarding the *R-peak - offset* method revealed, that subtracting 34 ms from the R-peak results in the best R-onset approximation. A MAE of 5.62 ms and a SD of 4.74 ms were found. The 40 ms published by van Lien et al. showed only the six best performance [Lie13], as the MAE was 8.78 ms and the SD was 6.43 ms. However, the R-onset and not the Q-onset was manually labeled in this work. Therefore, the accuracy of the proposed 40 ms could not be examined.

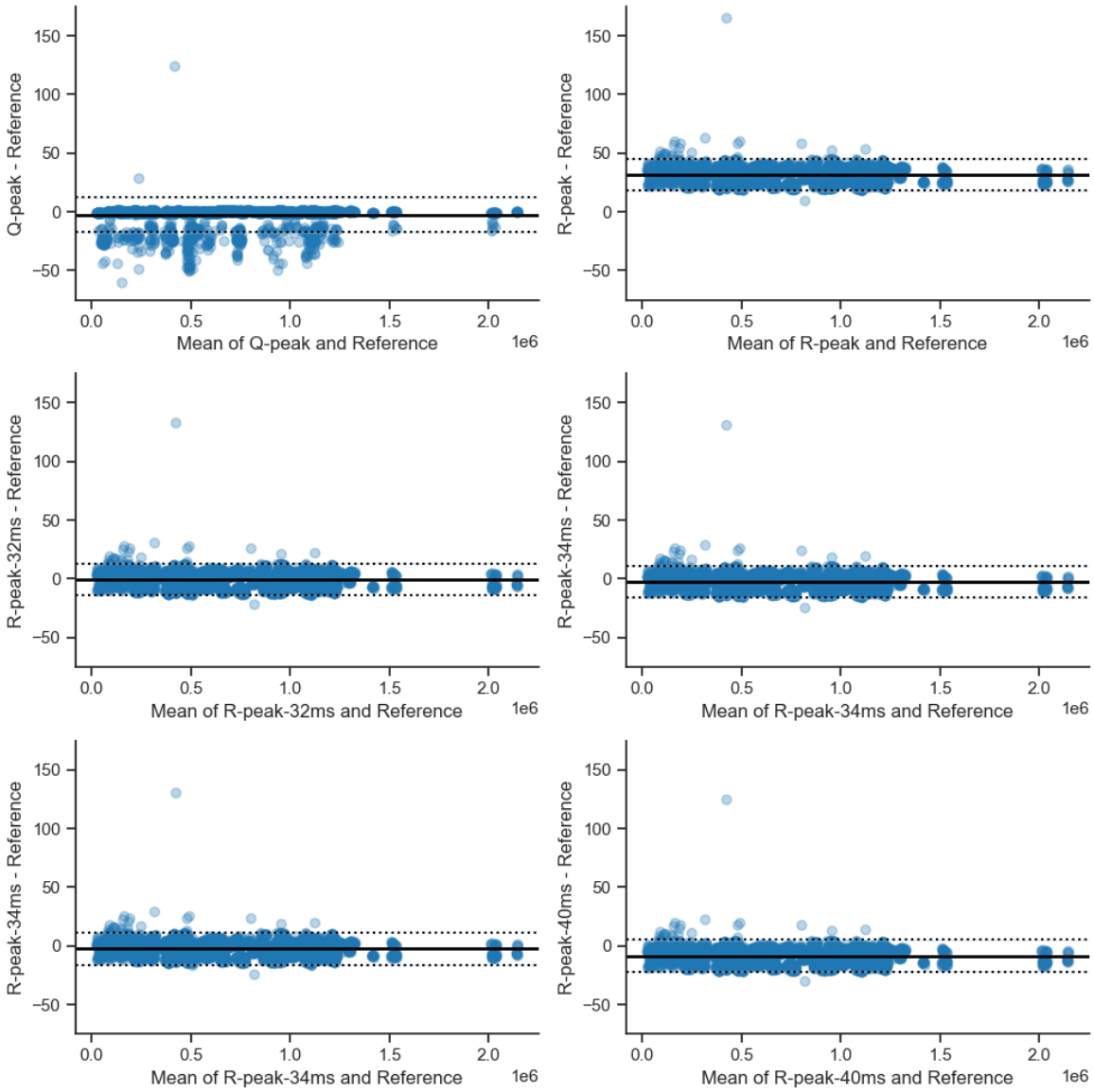

Figure 5.3: Residual plots of the most important Q-onset detection methods.

5.2.2 B-Point

Furthermore, the ability of the B-point detection algorithms to pinpoint the B-points with minimal deviation from the manually labeled reference data was also investigated in this work. As in the previous chapters, the MAE, ME, and Md were calculated with respect to the reference data. Since a detailed analysis of all results is not possible, the relevant ones are marked red in Table 5.6.

The best performance was achieved by the algorithm that fits a straight line between the C-point and the point 150 ms prior to the C-point, firstly. Afterward, the maximal vertical

Table 5.6: Overview of the performance of the B-point detection methods with regard to the manually labeled gold standard.

B-point detection	Outlier correction	MAE ± SD	ME ± SD	Md
Multiple conditions	—	23.51 ± 27.24	-21.82 ± 28.61	-10.0
	Autoregression	21.16 ± 23.68	-18.10 ± 26.09	-8.0
	Interpolation	20.65 ± 23.43	-17.05 ± 26.16	-8.0
Second derivative	—	17.09 ± 16.89	-5.22 ± 23.45	-10.0
	Autoregression	16.62 ± 16.78	-2.80 ± 23.45	-8.0
	Interpolation	17.15 ± 17.36	-0.26 ± 24.40	-8.0
Straight line	—	15.17 ± 15.70	9.66 ± 19.58	9.0
	Autoregression	15.49 ± 14.84	12.88 ± 17.15	10.0
	Interpolation	15.88 ± 15.25	13.80 ± 17.15	10.0
Third derivative	—	23.83 ± 18.82	18.88 ± 23.78	16.0
	Autoregression	25.45 ± 18.06	24.44 ± 19.40	19.0
	Interpolation	26.26 ± 18.40	25.44 ± 19.53	20.0

distance between the line and the dZ/dt signal was calculated, to obtain the B-point location. In this case a MAE of 15.17 ms with a SD of 15.70 ms could be achieved. With a MAE of 16.62 ms and an SD of 16.78 ms the pipeline based on the second derivative and an autoregressive model for outlier correction performed second best. This observation is also reflected in the MAE of total PEP, where the pipeline combining the previously described approach with the *R-peak - 40 ms* method achieved the lowest MAE.

Considering the performance of the algorithm, which was described as the best in related work, the result is consistent with the observations of the analysis of the PEP duration. A MAE of 21.16 ms and an SD of 23.68 ms indicate that this algorithm does not work as expected. When looking at the residual plot of the algorithm based on multiple conditions without outlier correction, which is illustrated in Figure 5.4, a clear tendency of the data in the negative y-direction can be observed. This can also be seen in the ME of -18.10 ms. As can be seen in Figure 5.4, the autoregressive model does lead to correcting some outliers but does not influence the mean value strongly enough in the positive y-direction. A possible explanation for this observation is, that the algorithm based on multiple decision rules clipped the B-point to the A-point when no significant features were detected in the search interval extracted before. Since the A-point occurs earlier than the B-point, a systematic underestimation is introduced in this case.

The assumption, that the systematic overestimation of the R-onset was compensated by a systematic overestimation of the B-point location by the algorithm combination, based on the third derivative and an outlier correction with linear interpolation, is confirmed through the results from this investigation. The positive ME of 25.44 ms and the positive offset in the residual plot (Figure 5.4) verify this assumption.

Regarding the outlier correction methods, a pattern can be observed. Whereas the outlier correction led to a decrease in the MAE for the methods based on multiple decision rules and the second derivative, the opposite was observed for the methods based on the straight line and the third derivative. Looking at the ME, it can be observed that the outlier correction improved the performance for the methods, that tend to underestimate the B-point location, while the opposite is observable for the algorithms that tend to overestimate the B-point location. These results are not consistent with the observations in the residual plots, as outliers were visibly moved in the direction of the mean line. A possible explanation for this discrepancy is the way in which outlier detection was carried out in this work. To be able to detect outliers, firstly, the B-point time data had to be obtained [For18]. For this purpose, the distance to the C-point was calculated. Accordingly, points that were far away from the C-point and thus appeared too early, were detected as outliers. However, when the B-point detection algorithm led to a systematic overestimation of the B-point location, the values that occurred early with regard to the other detected points were also shifted backward by the outlier correction method. This leads to a further shift of the data towards the C-point and consequently increases the overestimation and the mean absolute error accordingly. Therefore, the described outlier detection method, based on the distance to the C-point is only suitable for B-point detection algorithms that do not introduce a systematic overestimation of the B-point location.

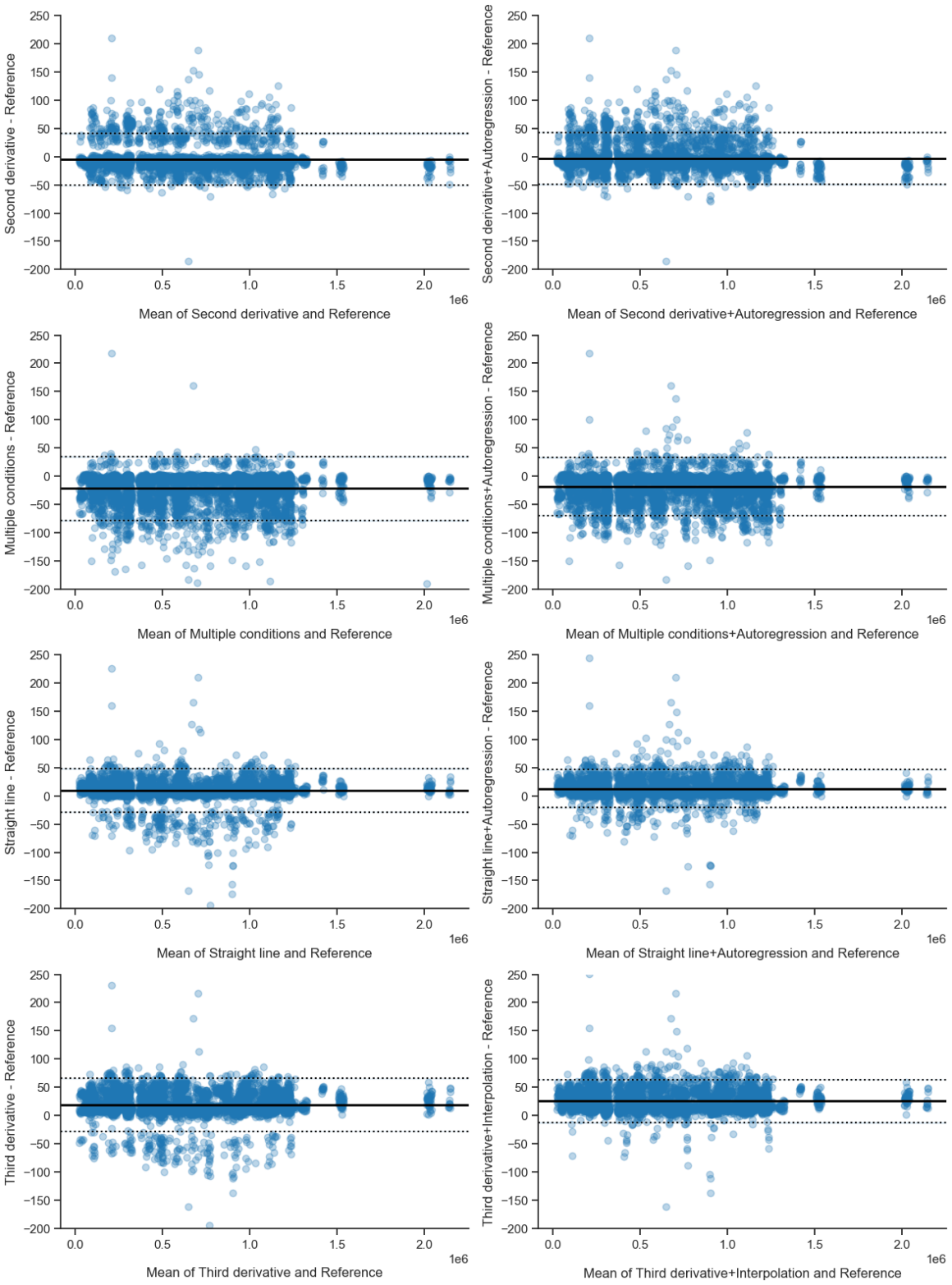

Figure 5.4: Comaparision of the B-point detection algorithms without outlier correction (left column) and with outlier correction (right column).

5.2.3 Best Performing Algorithm

The best-performing algorithm subtracted 40 ms from the R-peak to estimate the R-onset, and used the reversal point of the second derivative with an autoregressive model for B-point extraction. To verify whether a 40 ms time interval produces the best possible PEP outcomes, in combination with the B-point detection algorithm described above, the values of the time interval were varied between 30 ms and 50 ms. However, the pipeline with a constant time interval of 40 ms, which was used before showed the lowest MAE with respect to the reference data. An overview of the obtained results is provided in Table 5.7.

Table 5.7: Comparision of the performance of several fixed time intervals for PEP computation.

Q-onset	MAE ± SD	ME ± SD	Md
R-peak - 30 ms	17.73 ± 16.65	-4.43 ± 23.92	-9.0
R-peak - 32 ms	16.82 ± 17.18	-2.43 ± 23.92	-7.0
R-peak - 34 ms	16.12 ± 17.67	-0.43 ± 23.92	-5.0
R-peak - 36 ms	15.64 ± 18.16	1.57 ± 23.92	-3.0
R-peak - 38 ms	15.36 ± 18.67	3.57 ± 23.92	-1.0
R-peak - 40 ms	15.31 ± 19.20	5.57 ± 23.92	1.0
R-peak - 42 ms	15.50 ± 19.72	7.57 ± 23.92	3.0
R-peak - 44 ms	15.94 ± 20.24	9.57 ± 23.92	5.0
R-peak - 46 ms	16.66 ± 20.69	11.57 ± 23.92	7.0
R-peak - 48 ms	17.63 ± 21.10	13.57 ± 23.92	9.0
R-peak - 50 ms	18.83 ± 21.45	15.57 ± 23.92	11.0

Since the best-performing PEP computation pipeline was found, further investigations on whether the pipeline can detect changes in the individual's stress level were carried out. In alignment with the results obtained in the analysis of the reference PEP, a gap in mean PEP duration between the f-TSST and the TSST could be noticed (Table 5.8). However, the algorithm overestimates the actual PEP duration as can be seen in Figure 5.5.

Table 5.8: Overview of the MAE, ME, Md and mean PEP of the best-performing algorithm grouped by conditions.

Condition	MAE ± SD	ME ± SD	Md	PEPMean ± SD
f-TSST	15.51 ± 19.20	6.89 ± 23.71	1.0	99.49 ± 28.33
TSST	15.14 ± 19.19	4.40 ± 24.05	0.0	89.20 ± 29.14

The same can be observed on the phase level. Although there is a trend of overestimation of the PEP duration, which can be seen in Figure 5.6, and in the positive ME in Table 5.9, the relative changes between the phases are well reflected, which is also obtainable in Figure 5.6.

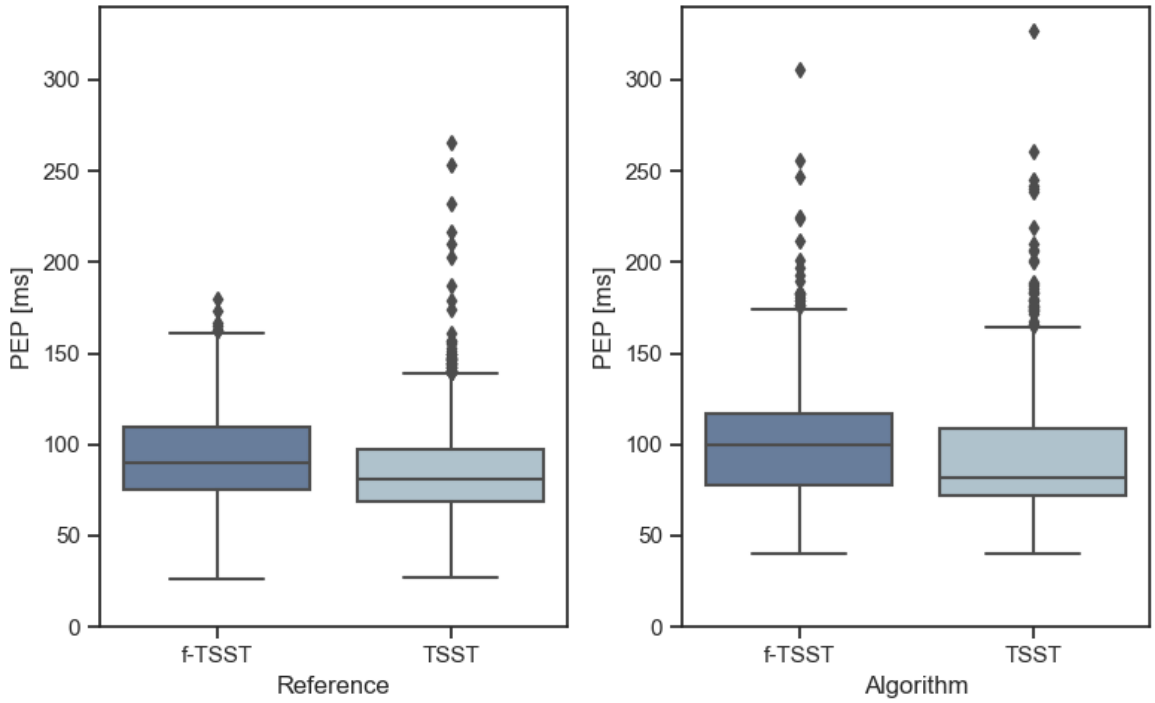

Figure 5.5: Comparision of the best-performing algorithm with the reference PEP on conditions level.

Table 5.9: Overview of the MAE, ME, Md and mean PEP of the best-performing algorithm grouped by phases.

Condition	Phase	MAE ± SD	ME ± SD	Md	PEP Mean ± SD
f-TSST	Prep	16.99 ± 20.34	7.22 ± 25.51	0.0	95.16 ± 27.59
	Pause_1	13.73 ± 14.39	3.22 ± 19.64	1.0	81.49 ± 26.09
	Talk	17.14 ± 21.20	9.50 ± 25.55	4.0	103.16 ± 27.96
	Math	14.72 ± 18.68	6.60 ± 22.85	1.0	101.71 ± 28.60
	Pause_5	9.67 ± 11.63	1.57 ± 15.06	-1.0	112.86 ± 21.14
TSST	Prep	16.57 ± 20.89	4.24 ± 26.33	-2.0	86.01 ± 30.78
	Pause_1	14.60 ± 18.52	1.42 ± 23.56	-3.0	78.85 ± 23.75
	Talk	18.22 ± 22.53	8.21 ± 27.80	2.0	93.86 ± 33.65
	Math	12.72 ± 15.24	3.22 ± 19.60	1.0	88.08 ± 23.77
	Pause_5	8.43 ± 7.22	-1.52 ± 11.01	-2.0	97.66 ± 23.12

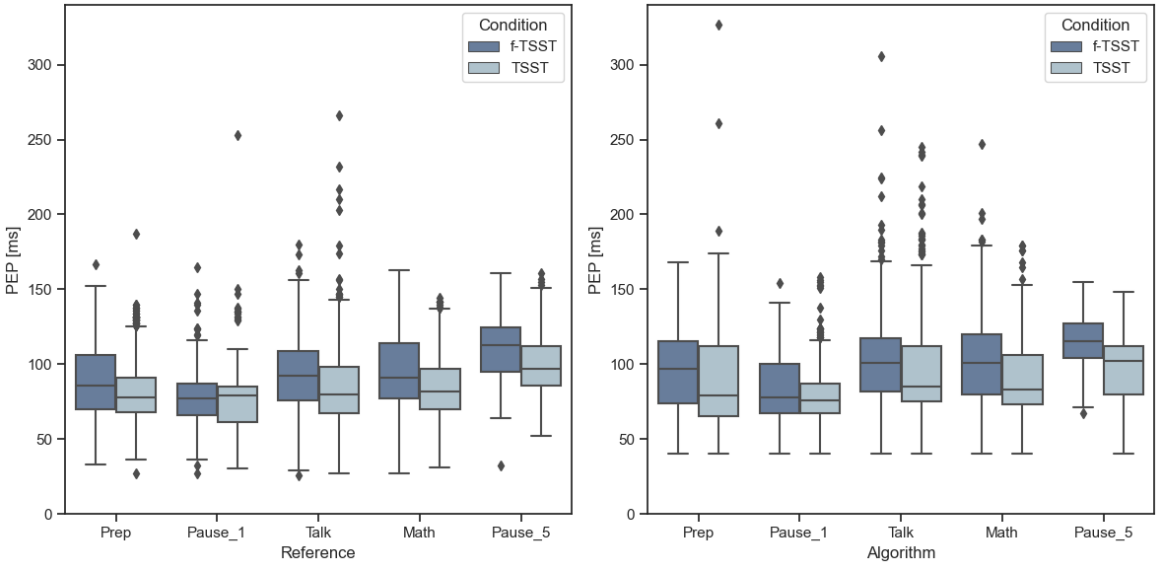

Figure 5.6: Comparision of the best-performing algorithm with the reference PEP on phase level.

The residual plot in Figure 5.7 provides information on the agreement between the PEP results obtained with the automatic algorithm and the manually labeled reference data. Consistent with the before mentioned findings, a slight overestimation of the PEP duration through the algorithm can be seen in a positive offset. Furthermore, a straight line can be identified, which seems to be the lower left border of the data. A possible explanation for this is, that the B-point was set to the R-peak, when no local minimum was found, in order to minimize the missing data for the outlier correction method. The residual plot in Figure 5.8, which shows the agreement of the algorithm discussed before without outlier correction confirms this assumption. No straight line can be seen in this plot, which is in line with the implementation. In the previously described scenario, the B-points were not set to the R-peak, but are considered to be undetected, when no outlier correction was performed afterward. The stretched shape of the plot with high point density near the mean line shows that the algorithm is able to reflect the reference data.

While absolute PEP levels are influenced by a variety of factors, PEP change may be more expressive, since they reflect the response to psychosocial stress induction independently of the baseline, which may vary between individual's [Ber04]. The results revealed that the algorithm is capable of reflecting these changes, which is quite promising.

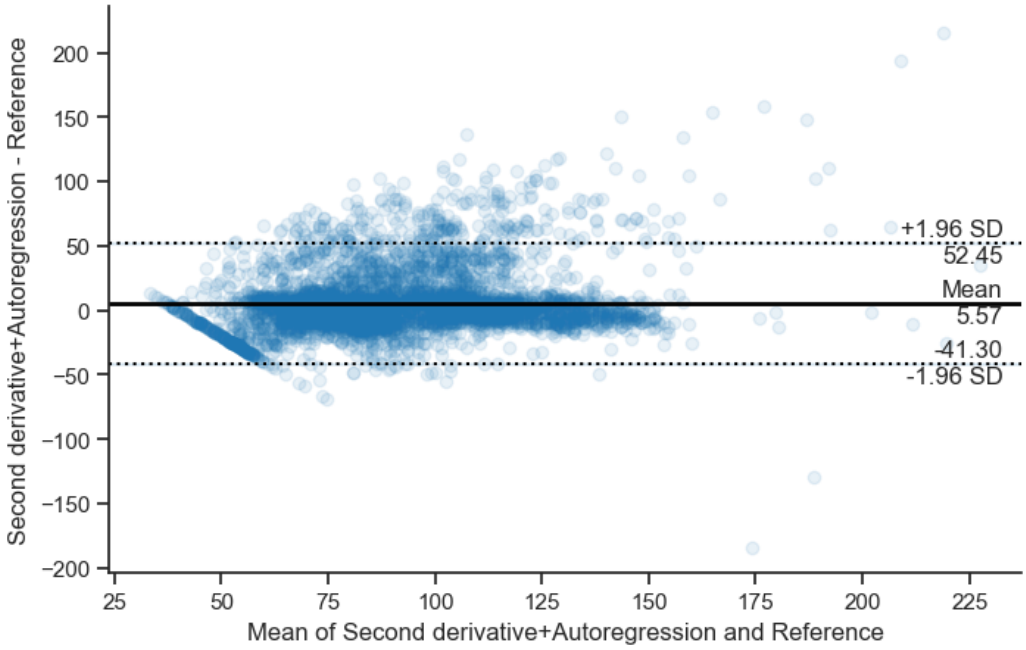

Figure 5.7: Residual plot of the manually labeled reference data and the best-performing algorithm.

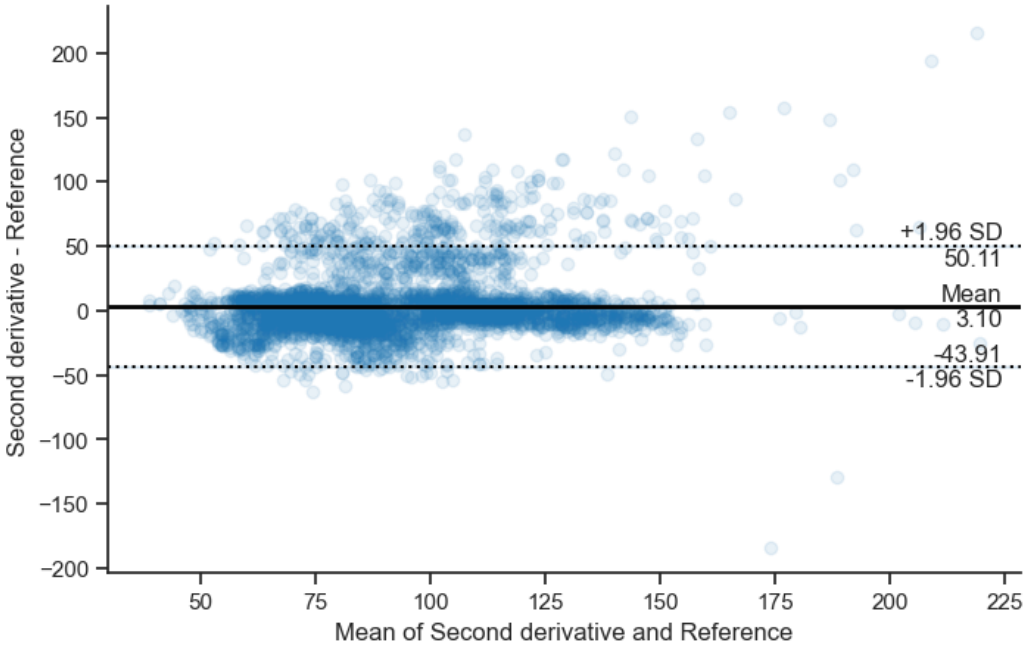

Figure 5.8: Residual plot of the manually labeled reference data and the best-performing algorithm without outlier correction.

5.3 General Discussions & Limitations

This bachelor thesis aimed to find out whether PEP is a valid marker for measuring changes in the human stress level caused by psychosocial stress induction. For this purpose, a total of 5086 cardiac cycles from all phases of the (f-)TSST, which was used for stress induction were labeled. The results of this work have shown, that PEP is able to reflect changes in the human stress level due to psychosocial stress induction, which is consistent with previous findings in related work [New79; Kro17].

Another goal of this bachelor thesis was, to investigate commonly used automatic B-point detection algorithms systematically. The necessity of such an investigation was shown by Arbol et al. [Árb17]. According to this 72% of the authors did not specify, which automatic B-point detection algorithm was used. Another 23% reported using Lozano's polynomial method, which did not provide reliable results in related work [Lie13; Árb17]. Therefore, a total of 36 different PEP computation pipelines were compared in terms of their performance with a manually labeled dataset, generated in this work. Apart from commonly used B-point detection methods based on the calculation of the reversal point in the $\boldsymbol{dZ^2/dt^2}$ signal [Deb93] or the maximum in the $\boldsymbol{dZ^3/dt^3}$ signal [Árb17], a method based on the vertical distance between a straight line reaching from the point 150 ms prior to the C-point to the C-point was implemented in this work [Dro22]. To the best of my knowledge, the performance of this algorithm has not yet been systematically investigated. In addition, an algorithm based on different decision rules, and thresholds to detect the B-point was implemented. This approach incorporates an outlier detection with subsequent correction, which was also applied to the other B-point detection algorithms [For18]. As an alternative outlier correction method, linear interpolation was performed, which is often used for data imputation [Lep17; Kul21]. The investigations have shown, that the PEP computation pipeline, based on subtracting a constant time interval of 40 ms to estimate the R-onset, and using the reversal point of the second derivative combined with an autoregressive model, to detect the B-point, showed superior performance. To achieve the highest accuracy in the isolated computation of the start and end points of PEP, the Q-peak detection algorithm and the method based on the straight line without outlier correction should be used as they showed the least mean absolute error from the reference data.

Since pinpointing the Q-wave onset was not possible for every participant, due to the lack of visible Q-waves, the R-onset had to be used as the start point of PEP, according to the recommendation of Bernston et al.. This ensured reliable labeling and a between-subject variance could be avoided [Ber04]. Even though relative changes in PEP may be of greater importance [Ber04], PEP could not be labeled according to the physiological definition [Pil23]. This represents a limitation of this work when absolute values should be compared with the results of other investigations.

Another limitation that could be an explanation for the poor performance of the algorithm, published by Forouzanfar et al., is the lack of a detailed description of some steps of the algorithm [For18]. Accordingly, assumptions had to be made in the implementation, which may have influenced the performance of the algorithm. With an accurate description, these inconsistencies could have been avoided and the results would have been more comparable.

Chapter 6

Conclusion & Outlook

In the context of this bachelor thesis, a reference dataset could be generated by manual labeling. A major strength of the dataset is that the 5086 labeled cardiac cycles contain data of all phases of the (f-)f-TSST. Thus, in addition to resting conditions, the data set also contains phases in which the participants were exposed to psychosocial stress. Therefore, this dataset can be used to validate the accuracy of PEP as a marker of psychosocial stress through comparison with gold standard stress markers. Additionally, this dataset provides the opportunity to systematically investigate the accuracy of commonly used event detection algorithms.

The results of this work revealed, that the reference dataset is able to reflect changes in the individual's stress level. A mean PEP difference of 8.43% between the TSST and the f-TSST, that served as a control condition, and the measured differences between the phases of the (f-)TSST underline this finding.

Furthermore, commonly used event detection algorithms were implemented and their accuracy was investigated with respect to the reference dataset. In total 36 event detection pipelines were examined. The application of the outlier correction, proposed by Forouzanfar et al. to all B-point detection algorithms has, to the best of my knowledge not been attempted before [For18]. However, the results were quite promising. Visual inspection of the residual plots showed, that both the autoregressive model and linear interpolation improved the results. This trend was not reflected in the mean absolute error for each inspected algorithm, due to inadequate outlier detection. Consequently, there is room for further improvements at this point.

The algorithm, described as the best algorithm in related work, showed a surprisingly poor performance in this work. A possible improvement of the algorithm could be achieved by limiting the search interval for the B-point detection. Forouzanfar et al. suggest to use the ECG signal to do so [For18]. The R-peak was used as the left border of the B-point search

interval, in the algorithm based on the reversal point of the $\boldsymbol{dZ^2/dt^2}$ signal in this work. This algorithm, combined with an outlier correction by an autoregressive model, produced the lowest MAE of 15.31 ms. Therefore, it might be interesting to use the R-peak as the left border of the previously described algorithm too. In addition, further investigations to verify whether the combination of the algorithm based on the second derivative and the algorithm proposed by Forouzanfar et al. modified with an adjusted search window leads to an overall improvement, should be carried out in the future [For18].

List of Figures

List of Tables

Bibliography

[Aka69] Hirotugu Akaike. “Fitting autoregressive models for prediction”. en. In: *Annals of the Institute of Statistical Mathematics* 21.1 (Dec. 1969), pp. 243–247. ISSN: 0020-3157, 1572-9052. DOI: 10.1007/BF02532251. URL: http://link.springer.com/10.1007/BF02532251 (visited on 05/01/2023).

[AL-15] Hussain AL-Ziarjawey. “Heart Rate Monitoring and PQRST Detection Based on Graphical User Interface with Matlab”. In: *International Journal of Information and Electronics Engineering* (2015). ISSN: 20103719. DOI: 10.7763/IJIEE.2015.V5.550. URL: http://www.ijiee.org/index.php?m=content&c=index&a=show&catid=52&id=602 (visited on 04/26/2023).

[All17] Andrew P. Allen, Paul J. Kennedy, Samantha Dockray, John F. Cryan, Timothy G. Dinan, and Gerard Clarke. “The Trier Social Stress Test: Principles and practice”. en. In: *Neurobiology of Stress* 6 (Feb. 2017), pp. 113–126. ISSN: 23522895. DOI: 10.1016/j.ynstr.2016.11.001. URL: https://linkinghub.elsevier.com/retrieve/pii/S2352289516300224 (visited on 04/25/2023).

[Árb17] Javier Rodríguez Árbol, Pandelis Perakakis, Alba Garrido, José Luis Mata, M. Carmen Fernández-Santaella, and Jaime Vila. “Mathematical detection of aortic valve opening (B point) in impedance cardiography: A comparison of three popular algorithms: Mathematical detection of aortic valve opening”. en. In: *Psychophysiology* 54.3 (Mar. 2017), pp. 350–357. ISSN: 00485772. DOI: 10.1111/psyp.12799. URL: https://onlinelibrary.wiley.com/doi/10.1111/psyp.12799 (visited on 01/20/2023).

[Bal18] Joel Balmer, Christopher Pretty, Shaun Davidson, Thomas Desaive, Shun Kamoi, Antoine Pironet, Philippe Morimont, Nathalie Janssen, Bernard Lambermont, Geoffrey M Shaw, and J Geoffrey Chase. “Pre-ejection period, the reason why the electrocardiogram Q-wave is an unreliable indicator of pulse wave initialization”. In: *Physiological Measurement* 39.9 (Sept. 2018), p. 095005. ISSN: 1361-6579. DOI: 10.1088/1361-6579/aada72. URL: https://iopscience.iop.org/article/10.1088/1361-6579/aada72 (visited on 04/12/2023).

[Ber04] Gary G. Berntson, David L. Lozano, Yun-Ju Chen, and John T. Cacioppo. "Where to Q in PEP". en. In: *Psychophysiology* 41.2 (Mar. 2004), pp. 333–337. ISSN: 0048-5772, 1469-8986. DOI: 10.1111/j.1469-8986.2004.00156.x. URL: https://onlinelibrary.wiley.com/doi/10.1111/j.1469-8986.2004.00156.x (visited on 04/12/2023).

[Bio23] Biopac. *MP160 Starter Systems | BIOPAC*. en-US. 2023. URL: https://www.biopac.com/product-category/research/systems/mp150-starter-systems/ (visited on 04/26/2023).

[Bry08] Lena Brydon, Katie O'Donnell, Caroline E. Wright, Andrew J. Wawrzyniak, Jane Wardle, and Andrew Steptoe. "Circulating Leptin and Stress-induced Cardiovascular Activity in Humans". en. In: *Obesity* 16.12 (Dec. 2008), pp. 2642–2647. ISSN: 19307381. DOI: 10.1038/oby.2008.415. URL: http://doi.wiley.com/10.1038/oby.2008.415 (visited on 04/18/2023).

[Cac94] John T. Cacioppo, Gary G. Berntson, Philip F. Binkley, Karen S. Quigley, Bert N. Uchino, and Annette Fieldstone. "Autonomic cardiac control. II. Noninvasive indices and basal response as revealed by autonomic blockades". en. In: *Psychophysiology* 31.6 (Nov. 1994), pp. 586–598. ISSN: 0048-5772, 1469-8986. DOI: 10.1111/j.1469-8986.1994.tb02351.x. URL: https://onlinelibrary.wiley.com/doi/10.1111/j.1469-8986.1994.tb02351.x (visited on 01/20/2023).

[Car15] Carlos Carreiras, Ana Priscila Alves, André Lourenço, Filipe Canento, Hugo Silva, Ana Fred, et al. *BioSPPy: Biosignal Processing in Python*. [Online; accessed <today>]. 2015. URL: https://github.com/PIA-Group/BioSPPy/.

[Chr04] Ivaylo I Christov. "Real time electrocardiogram QRS detection using combined adaptive threshold". en. In: *BioMedical Engineering OnLine* 3.1 (Dec. 2004), p. 28. ISSN: 1475-925X. DOI: 10.1186/1475-925X-3-28. URL: https://biomedical-engineering-online.biomedcentral.com/articles/10.1186/1475-925X-3-28 (visited on 04/29/2023).

[Cyb12] Gerard Cybulski, Anna Strasz, Wiktor Niewiadomski, and Anna Gąsiorowska. "Impedance cardiography: Recent advancements". In: *Cardiology Journal* 19.5 (Oct. 2012), pp. 550–556. ISSN: 1898-018X, 1897-5593. DOI: 10.5603/CJ.2012.0104. URL: http://czasopisma.viamedica.pl/cj/article/view/22977 (visited on 04/27/2023).

[Deb93] Thomas T. Debski, Yaxi Zhang, J.Richard Jennings, and Thomas W. Kamarck. "Stability of cardiac impedance measures: Aortic opening (B-point) detection and scoring". en. In: *Biological Psychology* 36.1-2 (Aug. 1993), pp. 63–74. ISSN:

03010511. DOI: 10.1016/0301-0511(93)90081-I. URL: https://linkinghub.elsevier.com/retrieve/pii/030105119390081I (visited on 04/11/2023).

[Doe21] Rumi Iqbal Doewes, Lekshmi Gangadhar, and Saranyadevi Subburaj. "An overview on stress neurobiology: Fundamental concepts and its consequences". en. In: *Neuroscience Informatics* 1.3 (Nov. 2021), p. 100011. ISSN: 27725286. DOI: 10.1016/j.neuri.2021.100011. URL: https://linkinghub.elsevier.com/retrieve/pii/S277252862100011X (visited on 01/20/2023).

[Dro22] L. Drost, J. B. Finke, J. Port, and H. Schächinger. "Comparison of TWA and PEP as indices of α2- and ß-adrenergic activation". en. In: *Psychopharmacology* 239.7 (July 2022), pp. 2277–2288. ISSN: 0033-3158, 1432-2072. DOI: 10.1007/s00213-022-06114-8. URL: https://link.springer.com/10.1007/s00213-022-06114-8 (visited on 01/20/2023).

[Emp23] EmpkinS. *Website of the CRC 1483 EmpkinS › EmpkinS*. de. 2023. URL: https://www.empkins.de/ (visited on 04/14/2023).

[For18] Mohamad Forouzanfar, Fiona C. Baker, Massimiliano de Zambotti, Corey McCall, Laurent Giovangrandi, and Gregory T. A. Kovacs. "Toward a better noninvasive assessment of preejection period: A novel automatic algorithm for B-point detection and correction on thoracic impedance cardiogram". en. In: *Psychophysiology* 55.8 (Aug. 2018), e13072. ISSN: 00485772. DOI: 10.1111/psyp.13072. URL: https://onlinelibrary.wiley.com/doi/10.1111/psyp.13072 (visited on 01/20/2023).

[For19] Mohamad Forouzanfar, Fiona C. Baker, Ian M. Colrain, Aimée Goldstone, and Massimiliano Zambotti. "Automatic analysis of pre-ejection period during sleep using impedance cardiogram". en. In: *Psychophysiology* 56.7 (July 2019), e13355. ISSN: 0048-5772, 1469-8986. DOI: 10.1111/psyp.13355. URL: https://onlinelibrary.wiley.com/doi/10.1111/psyp.13355 (visited on 04/29/2023).

[Hla05] Thinn Hlaing, Tara DiMino, Peter R. Kowey, and Gan-Xin Yan. "ECG Repolarization Waves: Their Genesis and Clinical Implications". en. In: *Annals of Noninvasive Electrocardiology* 10.2 (Apr. 2005), pp. 211–223. ISSN: 1542-474X, 1082-720X. DOI: 10.1111/j.1542-474X.2005.05588.x. URL: https://onlinelibrary.wiley.com/doi/10.1111/j.1542-474X.2005.05588.x (visited on 04/26/2023).

[Kay88] Steven M Kay. *Modern spectral estimation*. Pearson Education India, 1988.

[Kir93] Clemens Kirschbaum, Karl-Martin Pirke, and Dirk H. Hellhammer. "The 'Trier Social Stress Test' – A Tool for Investigating Psychobiological Stress Responses in a Laboratory Setting". en. In: *Neuropsychobiology* 28.1-2 (1993), pp. 76–81.

ISSN: 0302-282X, 1423-0224. DOI: 10.1159/000119004. URL: https://www.karger.com/Article/FullText/119004 (visited on 01/20/2023).

[Kor18] Minke C. Kortekaas, Marit H. N. van Velzen, Frank Grüne, Sjoerd P. Niehof, Robert J. Stolker, and Frank J. P. M. Huygen. "Small intra-individual variability of the pre-ejection period justifies the use of pulse transit time as approximation of the vascular transit". en. In: *PLOS ONE* 13.10 (Oct. 2018). Ed. by Rudolf Kirchmair, e0204105. ISSN: 1932-6203. DOI: 10.1371/journal.pone.0204105. URL: https://dx.plos.org/10.1371/journal.pone.0204105 (visited on 01/20/2023).

[Kro17] J. Krohova, B. Czippelova, Z. Turianikova, Z. Lazarova, I. Tonhajzerova, and M. Javorka. "Preejection Period as a Sympathetic Activity Index: a Role of Confounding Factors". en. In: *Physiological Research* (Aug. 2017), S265–S275. ISSN: 1802-9973, 0862-8408. DOI: 10.33549/physiolres.933682. URL: http://www.biomed.cas.cz/physiolres/pdf/2017/66_S265.pdf (visited on 01/20/2023).

[Kul21] Lattawit Kulanuwat, Chantana Chantrapornchai, Montri Maleewong, Papis Wongchaisuwat, Supaluk Wimala, Kanoksri Sarinnapakorn, and Surajate Boonya-aroonnet. "Anomaly Detection Using a Sliding Window Technique and Data Imputation with Machine Learning for Hydrological Time Series". en. In: *Water* 13.13 (July 2021), p. 1862. ISSN: 2073-4441. DOI: 10.3390/w13131862. URL: https://www.mdpi.com/2073-4441/13/13/1862 (visited on 04/11/2023).

[Lab70] Zuhdi Lababidi, D. A. Ehmke, Robert E. Durnin, Paul E. Leaverton, and Ronald M. Lauer. "The First Derivative Thoracic Impedance Cardiogram". en. In: *Circulation* 41.4 (Apr. 1970), pp. 651–658. ISSN: 0009-7322, 1524-4539. DOI: 10.1161/01.CIR.41.4.651. URL: https://www.ahajournals.org/doi/10.1161/01.CIR.41.4.651 (visited on 04/21/2023).

[Lep17] Mathieu Lepot, Jean-Baptiste Aubin, and François Clemens. "Interpolation in Time Series: An Introductive Overview of Existing Methods, Their Performance Criteria and Uncertainty Assessment". en. In: *Water* 9.10 (Oct. 2017), p. 796. ISSN: 2073-4441. DOI: 10.3390/w9100796. URL: http://www.mdpi.com/2073-4441/9/10/796 (visited on 04/11/2023).

[Lie13] René van Lien, Nienke M. Schutte, Jan H. Meijer, and Eco J.C. de Geus. "Estimated preejection period (PEP) based on the detection of the R-wave and dZ/dt-min peaks does not adequately reflect the actual PEP across a wide range of laboratory and ambulatory conditions". en. In: *International Journal of Psychophysiology* 87.1 (Jan. 2013), pp. 60–69. ISSN: 01678760. DOI: 10.1016/j.ijpsycho.2012.11.001.

URL: https://linkinghub.elsevier.com/retrieve/pii/S0167876012006460 (visited on 01/20/2023).

[Loz07] David L. Lozano, Greg Norman, Dayan Knox, Beatrice L. Wood, Bruce D. Miller, Charles F. Emery, and Gary G. Berntson. "Where to B in dZ/dt". en. In: *Psychophysiology* 44.1 (Jan. 2007). ISSN: 0048-5772, 1469-8986. DOI: 10.1111/j.1469-8986.2006.00468.x. URL: https://onlinelibrary.wiley.com/doi/10.1111/j.1469-8986.2006.00468.x (visited on 04/20/2023).

[Lüt05] Helmut Lütkepohl. "Estimation of VARMA Models". en. In: *New Introduction to Multiple Time Series Analysis*. Berlin, Heidelberg: Springer Berlin Heidelberg, 2005, pp. 447–492. ISBN: 978-3-540-40172-8 978-3-540-27752-1. DOI: 10.1007/978-3-540-27752-1_12. URL: http://link.springer.com/10.1007/978-3-540-27752-1_12 (visited on 05/01/2023).

[Mak21] Dominique Makowski, Tam Pham, Zen J. Lau, Jan C. Brammer, François Lespinasse, Hung Pham, Christopher Schölzel, and S. H. Annabel Chen. "NeuroKit2: A Python toolbox for neurophysiological signal processing". In: *Behavior Research Methods* 53.4 (Feb. 2021), pp. 1689–1696. DOI: 10.3758/s13428-020-01516-y.

[Mal20] Mohsen Maleki, Mohammad Reza Mahmoudi, Darren Wraith, and Kim-Hung Pho. "Time series modelling to forecast the confirmed and recovered cases of COVID-19". en. In: *Travel Medicine and Infectious Disease* 37 (Sept. 2020), p. 101742. ISSN: 14778939. DOI: 10.1016/j.tmaid.2020.101742. URL: https://linkinghub.elsevier.com/retrieve/pii/S1477893920302210 (visited on 05/01/2023).

[Man18] Sofienne Mansouri, Tareq Alhadidi, Souhir Chabchoub, and R Ben Salah. "Impedance cardiography: recent applications and developments". In: *Biomed Res* 29.19 (2018), pp. 3542–3552.

[Mar15] Agnese Mariotti. "The effects of chronic stress on health: new insights into the molecular mechanisms of brain–body communication". en. In: *Future Science OA* 1.3 (Nov. 2015), fso.15.21. ISSN: 2056-5623. DOI: 10.4155/fso.15.21. URL: https://www.future-science.com/doi/10.4155/fso.15.21 (visited on 01/20/2023).

[McE17] Bruce S. McEwen. "Neurobiological and Systemic Effects of Chronic Stress". en. In: *Chronic Stress* 1 (Feb. 2017), p. 247054701769232. ISSN: 2470-5470, 2470-5470. DOI: 10.1177/2470547017692328. URL: http://journals.sagepub.com/doi/10.1177/2470547017692328 (visited on 04/24/2023).

[McS03] P.E. McSharry, G.D. Clifford, L. Tarassenko, and L.A. Smith. "A dynamical model for generating synthetic electrocardiogram signals". en. In: *IEEE Transactions on Biomedical Engineering* 50.3 (Mar. 2003), pp. 289–294. ISSN: 0018-9294. DOI: 10.1109/TBME.2003.808805. URL: http://ieeexplore.ieee.org/document/1186732/ (visited on 04/27/2023).

[Mei07] J.H. Meijer, S. Boesveldt, E. Elbertse, and H.W. Berendse. "Using time interval parameters from impedance cardiography to evaluate autonomic nervous function in Parkinson's disease". en. In: *13th International Conference on Electrical Bioimpedance and the 8th Conference on Electrical Impedance Tomography*. Ed. by Hermann Scharfetter and Robert Merwa. Vol. 17. Series Title: IFMBE Proceedings. Berlin, Heidelberg: Springer Berlin Heidelberg, 2007, pp. 596–599. ISBN: 978-3-540-73840-4. DOI: 10.1007/978-3-540-73841-1_154. URL: http://link.springer.com/10.1007/978-3-540-73841-1_154 (visited on 04/20/2023).

[Nag89] J. H. Nagel, L. Y. Shyu, S. P. Reddy, B. E. Hurwitz, P. M. McCabe, and N. Schneiderman. "New signal processing techniques for improved precision of noninvasive impedance cardiography". en. In: *Annals of Biomedical Engineering* 17.5 (Sept. 1989), pp. 517–534. ISSN: 0090-6964, 1573-9686. DOI: 10.1007/BF02368071. URL: http://link.springer.com/10.1007/BF02368071 (visited on 01/31/2023).

[New79] David B. Newlin and Robert W. Levenson. "Pre-ejection Period: Measuring Beta-adrenergic Influences Upon the Heart". en. In: *Psychophysiology* 16.6 (Nov. 1979), pp. 546–552. ISSN: 0048-5772, 1469-8986. DOI: 10.1111/j.1469-8986.1979.tb01519.x. URL: https://onlinelibrary.wiley.com/doi/10.1111/j.1469-8986.1979.tb01519.x (visited on 04/15/2023).

[Oll22] Malte Ollenschläger, Arne Küderle, Wolfgang Mehringer, Ann-Kristin Seifer, Jürgen Winkler, Heiko Gaßner, Felix Kluge, and Bjoern M. Eskofier. "MaD GUI: An Open-Source Python Package for Annotation and Analysis of Time-Series Data". en. In: *Sensors* 22.15 (Aug. 2022), p. 5849. ISSN: 1424-8220. DOI: 10.3390/s22155849. URL: https://www.mdpi.com/1424-8220/22/15/5849 (visited on 04/28/2023).

[Pil23] Niklas Pilz, Andreas Patzak, and Tomas L. Bothe. "The pre-ejection period is a highly stress dependent parameter of paramount importance for pulse-wave-velocity based applications". In: *Frontiers in Cardiovascular Medicine* 10 (Feb. 2023), p. 1138356. ISSN: 2297-055X. DOI: 10.3389/fcvm.2023.1138356. URL:

https://www.frontiersin.org/articles/10.3389/fcvm.2023.1138356/full (visited on 04/15/2023).

[Raf21] Nikita Rafie, Anthony H. Kashou, and Peter A. Noseworthy. "ECG Interpretation: Clinical Relevance, Challenges, and Advances". en. In: *Hearts* 2.4 (Nov. 2021), pp. 505–513. ISSN: 2673-3846. DOI: 10.3390/hearts2040039. URL: https://www.mdpi.com/2673-3846/2/4/39 (visited on 04/26/2023).

[Sam15] Michael Sampson and Anthony McGrath. "Understanding the ECG Part 2: ECG basics". en. In: *British Journal of Cardiac Nursing* 10.12 (Dec. 2015), pp. 588–594. ISSN: 1749-6403, 2052-2207. DOI: 10.12968/bjca.2015.10.12.588. URL: http://www.magonlinelibrary.com/doi/10.12968/bjca.2015.10.12.588 (visited on 04/26/2023).

[Sea10] Skipper Seabold and Josef Perktold. "statsmodels: Econometric and statistical modeling with python". In: *9th Python in Science Conference*. 2010.

[See16] Mark D. Seery, Cheryl L. Kondrak, Lindsey Streamer, Thomas Saltsman, and Veronica M. Lamarche. "Preejection period can be calculated using R peak instead of Q". en. In: *Psychophysiology* 53.8 (Aug. 2016), pp. 1232–1240. ISSN: 0048-5772, 1469-8986. DOI: 10.1111/psyp.12657. URL: https://onlinelibrary.wiley.com/doi/10.1111/psyp.12657 (visited on 04/11/2023).

[Sha19] Md Mobashir Hasan Shandhi, Beren Semiz, Sinan Hersek, Nazli Goller, Farrokh Ayazi, and Omer T. Inan. "Performance Analysis of Gyroscope and Accelerometer Sensors for Seismocardiography-Based Wearable Pre-Ejection Period Estimation". In: *IEEE Journal of Biomedical and Health Informatics* 23.6 (Nov. 2019), pp. 2365–2374. ISSN: 2168-2194, 2168-2208. DOI: 10.1109/JBHI.2019.2895775. URL: https://ieeexplore.ieee.org/document/8627923/ (visited on 01/20/2023).

[She22] Shafa-at Ali Sheikh, Nil Z. Gurel, Shishir Gupta, Ikenna V. Chukwu, Oleksiy Levantsevych, Mhmtjamil Alkhalaf, Majd Soudan, Rami Abdulbaki, Ammer Haffar, Viola Vaccarino, Omer T. Inan, Amit J. Shah, Gari D. Clifford, and Ali Bahrami Rad. "Data-driven approach for automatic detection of aortic valve opening: B point detection from impedance cardiogram". en. In: *Psychophysiology* 59.12 (Dec. 2022). ISSN: 0048-5772, 1469-8986. DOI: 10.1111/psyp.14128. URL: https://onlinelibrary.wiley.com/doi/10.1111/psyp.14128 (visited on 04/21/2023).

[She90] Andrew Sherwood(Chair), Michael T. Allen, Jochen Fahrenberg, Robert M. Kelsey, William R. Lovallo, and Lorenz J.P. Doornen. "Methodological Guidelines for Impedance Cardiography". en. In: *Psychophysiology* 27.1 (Jan. 1990), pp. 1–23.

ISSN: 0048-5772, 1469-8986. DOI: 10.1111/j.1469-8986.1990.tb02171.x. URL: https://onlinelibrary.wiley.com/doi/10.1111/j.1469-8986.1990.tb02171.x (visited on 01/20/2023).

[Ste23] Ulla Sternemann. "Extraction of Pre-Ejection Period as Marker for Acute Psychosocial Stress from Wearable Sensors and Interferometry Radar". English. MA thesis. Erlangen: Friedrich-Alexander-Universität Erlangen-Nürnberg (FAU), Feb. 2023.

[tea20] The pandas development team. *pandas-dev/pandas: Pandas*. Version 1.5.3. Feb. 2020. DOI: 10.5281/zenodo.3509134. URL: https://doi.org/10.5281/zenodo.3509134.

[Vir20] Pauli Virtanen et al. "SciPy 1.0: fundamental algorithms for scientific computing in Python". en. In: *Nature Methods* 17.3 (Mar. 2020), pp. 261–272. ISSN: 1548-7091, 1548-7105. DOI: 10.1038/s41592-019-0686-2. URL: http://www.nature.com/articles/s41592-019-0686-2 (visited on 04/29/2023).

[Wie13] Uta S. Wiemers, Daniela Schoofs, and Oliver T. Wolf. "A friendly version of the Trier Social Stress Test does not activate the HPA axis in healthy men and women". en. In: *Stress* 16.2 (Mar. 2013), pp. 254–260. ISSN: 1025-3890, 1607-8888. DOI: 10.3109/10253890.2012.714427. URL: http://www.tandfonline.com/doi/full/10.3109/10253890.2012.714427 (visited on 01/20/2023).

[Wil96] Gonneke H. M. Willemsen, Eco J. C. DeGeus, Coert H. A. M. Klaver, Lorenz J. P. VanDoornen, and Douglas Carrofl. "Ambulatory monitoring of the impedance cardiogram". en. In: *Psychophysiology* 33.2 (Mar. 1996), pp. 184–193. ISSN: 0048-5772, 1469-8986. DOI: 10.1111/j.1469-8986.1996.tb02122.x. URL: https://onlinelibrary.wiley.com/doi/10.1111/j.1469-8986.1996.tb02122.x (visited on 04/18/2023).

Appendix A

Acronyms

SNS sympathetic nervous system

PNS parasympathetic nervous system

DBP diastolic blood pressure

HPA Hypothalamus-pituitary-adrenal

HR heart rate

HRV heart rate variability

PEP Pre-Ejection Period

ECG electrocardiogram

ICG impedance cardiogram

dZ/dt first derivative of the cardiac impedance

$\boldsymbol{dZ^2/dt^2}$ second derivative of the cardiac impedance

$\boldsymbol{dZ^3/dt^3}$ third derivative of the cardiac impedance

Q-onset Q-wave onset

R-onset R-wave onset

ISTI Initial Systolic Time Interval

TSST Trier Social Stress Test

f-TSST control version of the Trier Social Stress Test

FIR finite impulse response

DWT discrete wavelet transform

ARIMA Autoregressive Integrated Moving Average

AIC Akaike information criterion

ME mean error

MAE mean absolute error

Md median

SD standard deviation